

Optimization Perspective on Raking

Ariane Ducellier^{1*}, Alexander Hsu^{1,2}, Parkes Kendrick¹, Bill Gustavson¹,
 Laura Dwyer-Lindgren¹, Christopher Murray¹, Peng Zheng¹,
 and Aleksandr Aravkin^{1,2}

¹Institute for Health Metrics and Evaluation, University of Washington

²Department of Applied Mathematics, University of Washington

May 12, 2025

Abstract

Raking is widely used in survey inference and global health models to adjust the observations in contingency tables to given marginals, in the latter case reconciling estimates between models with different granularities. We review the convex optimization foundation of raking and focus on a dual perspective that simplifies and streamlines prior raking extensions and provides new functionality, enabling a unified approach to n -dimensional raking, raking with differential weights, ensuring bounds on estimates are respected, raking to margins either as hard constraints or as aggregate observations, handling missing data, and allowing efficient uncertainty propagation. The dual perspective also enables a uniform fast and scalable matrix-free optimization approach for all of these extensions. All of the methods are implemented in an open source Python package with an intuitive user interface, installable from PyPi¹, and we illustrate the capabilities using synthetic data and real mortality estimates.

Keywords: raking, convex optimization, global health estimates, uncertainty quantification

*The authors gratefully acknowledge the Bill and Melinda Gates Foundation

¹<https://pypi.org/project/raking/>

1 Introduction

We review the historical context of the raking problem in survey sciences and global health, and highlight connections to optimization through the iterative proportional fitting (IPF) algorithm. We also present convex analysis preliminaries that are used to develop the contributions in the paper.

1.1 Historical Context

Raking originated in survey inference, where it was used to adjust the sampling weights of the cases in a contingency table in order to match the marginal totals of the adjusted weights to the corresponding totals for the population (cf. Tillé (2020)). Given a population \mathcal{U} we want the population total of a variable Y , $\mathcal{Y} = \sum_{i \in \mathcal{U}} y_i$, estimated using a sample $S \subseteq \mathcal{U}$. Let π_i denote the inclusion probability of individual i into the sample, and let $d_i = \frac{1}{\pi_i}$. The classic Horvitz–Thompson–Narain estimator for \mathcal{Y} (Narain (1951); Horvitz and Thompson (1952)) is given by

$$\hat{\mathcal{Y}} = \sum_{i \in S} \frac{y_i}{\pi_i} = \sum_{i \in S} d_i y_i. \quad (1)$$

We may also have access to information on k auxiliary variables. We define by $x_i \in \mathbb{R}^k$ the vector of the values taken by the k auxiliary variables for an individual i . While individual auxiliary vectors are unknown, suppose we have the marginal sum $s \in \mathbb{R}^k$ from the population \mathcal{U} . The goal of raking in survey science is to replace the weights d_i in (1) by raking weights w_i such that

$$\sum_{i \in S} w_i x_i = s,$$

and use these to compute an estimate of $\mathcal{Y} = \sum_{i \in S} w_i y_i$ with associated uncertainty.

The formulations and goals of raking in global health research are different. We consider the sample S to be the population \mathcal{U} , and adjust the values taken by the y_i so their sum is equal to the known total s , which may come from a trusted data source or model of

lower granularity. To map this case to the above framework, the weights d_i are identically equal to 1, while auxiliary variables x are different margins over \mathcal{U} . For example, in one-dimensional raking, there is a single auxiliary variable and corresponding marginal total $\sum_{i \in \mathcal{U}} x_i = s$. In 2-dimensional raking, auxiliary variables are row and column sums of Y , with corresponding marginal vector s . In all cases, rather than looking for raking weights w_i , we are interested in directly finding the raked values $\beta_i = w_i y_i$.

1.2 Raking and the Iterative Proportional Fitting (IPF) Algorithm

A key connection to optimization appears in two-dimensional raking, when we are given linear combinations of the data (e.g. n row sums and m column sums) as constraints. We then have $k = m + n$ auxiliary variables. The raking problem now takes the form

$$\min_{\beta} f(\beta; y) \quad \text{s.t.} \quad \beta \mathbf{1}_n = s_r \text{ and } \beta^T \mathbf{1}_m = s_c, \quad (2)$$

where $\beta, y \in \mathbb{R}^{m \times n}$, $s_r \in \mathbb{R}^m$ and $s_c \in \mathbb{R}^n$. The iterative proportional fitting (IPF) algorithm, an algorithm to solve (2) with f the entropic distance function

$$f(\beta; y) = \sum_{i=1}^m \sum_{j=1}^n \beta_{i,j} \log \left(\frac{\beta_{i,j}}{y_{i,j}} \right) - (\beta_{i,j} - y_{i,j}) \quad (3)$$

was first proposed by Deming and Stephan (1940) and further developed by Stephan (1942), though these early works focused on the iterative raking procedure rather than the underlying formulation (2)-(3). The calibration method was further developed by Deville and Särndal (1992) and Deville et al. (1993) to adjust samples on known population totals. A review of the method and optimization formulations is found in Devaud and Tillé (2019), with the exception of the explicit dual and primal-dual relationships developed here.

A great reference to the IPF method itself from an optimization perspective is provided by She and Tang (2019). IPF and the equivalent, the Sinkhorn iteration (Sinkhorn (1967)) take advantage of block-separable constraints for rows and columns to obtain efficient

primal-dual updates in 2D raking and related problems, such as optimal transport (Cuturi (2013)). In the current paper, we show that the same underlying structure can be used in simple direct methods, such as Newton, to solve the dual just as efficiently. This allows us to focus on generalizing the model to apply to extended use cases, such as inexact observations rather than marginal constraints (Williams and Savitsky (2024)), to forego the development of modified IPF algorithms and to rely on the sparsity of the underlying linear operators to maintain computational efficiency.

In the next section we review convex analysis preliminaries that we rely on throughout the methods section.

1.3 Convex Preliminaries

We present selected topics from convex analysis that we need to frame the dual perspective on raking. For a canonical reference that goes much deeper into these ideas, please see Rockafellar and Wets (2009).

For a function $f : \mathbb{R}^p \rightarrow \overline{\mathbb{R}} := \mathbb{R} \cup \{-\infty, \infty\}$, define the *epigraph*

$$\text{epi}(f) = \{(\beta, \alpha) : f(\beta) \leq \alpha\} \subset \mathbb{R}^{p+1}. \quad (4)$$

A function $f : \mathbb{R}^p \rightarrow \overline{\mathbb{R}}$ is *closed* when $\text{epi}(f)$ is a closed set, *proper* when $f \not\equiv \infty$ and does not take the value of $-\infty$, and *convex* when $\text{epi}(f)$ is a convex set.

1.3.1 Convex Conjugate

For any function $f : \mathbb{R}^p \rightarrow \overline{\mathbb{R}}$, its *convex conjugate* is defined by

$$f^*(z) = \sup_{\beta} z^T \beta - f(\beta). \quad (5)$$

From the definition, *Fenchel's inequality* is immediate:

$$f(\beta) + f^*(z) \leq z^T \beta \quad \forall \beta, z. \quad (6)$$

For closed convex f , we have $f^{**} = f$, and we can write

$$f(\beta) = f^{**}(\beta) = \sup_z z^T \beta - f^*(z). \quad (7)$$

When f and f^* are differentiable, and we have attainment in the defining equation (6), we can differentiate each equality to get a key relationship between ∇f and ∇f^* :

$$z = \nabla_{\beta} f(\beta), \quad \beta = \nabla_z f^*(z) \quad \Rightarrow \quad \nabla_z f^*(\cdot) = \nabla_{\beta} f(\cdot)^{-1}. \quad (8)$$

For practical computation, the following basic identity relates conjugates of linear transforms of f to linear transforms of f^* :

$$(cf((\beta - a)/b))^*(z) = cf^*(bz/c) + az. \quad (9)$$

Finally, conjugates of separable functions are separable:

$$f(\beta) = \sum_i f_i(\beta_i) \quad \Rightarrow \quad f^*(z) = \sum_i f_i^*(z_i). \quad (10)$$

1.3.2 Convex Duality

The notion of *convex duality* is closely related to conjugacy. Given any convex program

$$\mathcal{P} : \quad \inf_{\beta} f(\beta) + g(A\beta - b) + c^T \beta \quad (11)$$

where f, g are closed proper convex functions, we can associate a saddle point system by writing g in terms of its conjugate (7):

$$g(A\beta - b) = g^{**}(A\beta - b) = \sup_{\lambda} \lambda^T (A\beta - b) - g^*(\lambda).$$

Substituting into (11), we define the resulting object as the Lagrangian:

$$\mathcal{L}(\beta, \lambda) := f(\beta) + c^T \beta + \lambda^T (A\beta - b) - g^*(\lambda). \quad (12)$$

While the primal is obtained by taking $\sup_{\lambda} \mathcal{L}(\beta, \lambda)$, we can compute the dual by interchanging the order and taking the infimum first:

$$\begin{aligned}
\mathcal{D} : \quad & \sup_{\lambda} \inf_{\beta} f(\beta) + c^T \beta + \lambda^T (A\beta - b) - g^*(\lambda) \\
& = \sup_{\lambda} -\lambda^T b - g^*(\lambda) - \sup_{\beta} (-c - A^T \lambda)^T \beta - f(\beta) \\
& = \sup_{\lambda} -\lambda^T b - g^*(\lambda) - f^*(-c - A^T \lambda).
\end{aligned} \tag{13}$$

Interchanging the order of optimization means the primal value is greater than or equal to the dual value. Simple technical conditions guarantee equality of primal and dual values and allow for optimal solutions to be characterized by simple equations and inequalities Rockafellar and Wets (2009). We focus on the relevant case in the next section.

1.3.3 Differentiable Objective with Equality Constraints

For the special case when f and f^* are differentiable and g encodes equality constraints, we can take

$$g(u) = \delta_0(u) = \begin{cases} 0 & u = 0 \\ \infty & u \neq 0. \end{cases}$$

The conjugate of the indicator function to 0 is then given by

$$g^*(z) = \sup_u u^T z - g(u) = 0.$$

That means the dual program (13) simplifies to

$$\sup_{\lambda} -\lambda^T b - f^*(-c - A^T \lambda) \quad \Leftrightarrow \quad \min_{\lambda} \lambda^T b + f^*(-c - A^T \lambda), \tag{14}$$

where we have written the dual as a minimization problem for convenience. The dual objective in the latter variant is smooth and convex, and the dual is unconstrained. Moreover, the Lagrangian (12) simplifies to

$$\mathcal{L}(\beta, \lambda) = f(\beta) + c^T \beta + \lambda^T (A\beta - b)$$

and we can obtain primal-dual relationships by differentiating the Lagrangian:

$$\nabla_{\beta} f(\beta^*) + c + A^T \lambda^* = 0 \quad \Rightarrow \quad \beta^* = (\nabla_{\beta} f)^{-1}(-c - A^T \lambda^*) = \nabla_z f^*(-c - A^T \lambda^*), \quad (15)$$

where we have used (8) to pass from the inverse of the gradient map to the gradient of the conjugate. Thus once we solve the dual, we can recover the primal solution simply by evaluating the gradient of the conjugate, regardless of the form of f .

1.4 Contributions

We revisit convex formulations of raking, as this perspective undergirds classic results and allows further extensions. Our goal is to provide a tool that is efficient for different problem dimensions, allows differential weighting to enable certainty of inputs to affect results, and provides different loss functions (deviances) of practical interest (Deville and Särndal (1992)) including raking of bounded values. The framework also incorporates aggregated observations of Williams and Savitsky (2024), useful when aggregates are noisy and uncertain.

Many of these extensions were gathered by Williams and Savitsky (2024). A key contribution of the current paper is to bring to light the form and structure of the dual problem and to use it for improved understanding, fast algorithms, and more challenging cases. Duality is an essential ingredient in efficient algorithms, particularly for higher dimensions. The dual perspective also brings clarity on the impact of missing data, and allows new methods of uncertainty propagation.

For smooth losses, duality allows the unique efficiency of the Iterative Proportional Fitting method to generalize to a variety of raking problems, leveraging a uniform matrix-free method such as Newton with a Minres subsolver. This enables raking at scale, which is essential for many of our use cases. The case of non-smooth loss is briefly discussed in Appendix A.6 but is not a focus of the paper.

In the global health context, when raking modeled estimates, efficient uncertainty propagation is a key consideration beyond computing the raked point estimate. We use the implicit function theorem to design a specialized delta method for raking, efficiently propagating uncertainty from both observations and aggregates for the smooth loss case.

The raking methods and extensions currently support applications within the Global Burden of Disease framework. We illustrate each case in Appendix B and also explain the interface to the open source tool used to implement all the methods².

2 Methods

We develop the general optimization perspective on raking and show how to use it to extend capabilities of the classic approach. We first review classic results that build intuition about entropic distance in the 1D case in Section 2.1 and the IPF algorithm for 2D raking in Section 2.2. We then discuss high-dimensional raking in Section 2.3, options for raking loss in Section 2.4, raking with weights in Section 2.5, using aggregates as observations rather than constraints in Section 2.6, strategies for missing data in Section 2.7, and efficient uncertainty quantification in Section 2.8.

2.1 1-D Raking from the Convex Analysis Perspective

We consider the classic one-dimensional case that motivates the use of entropic distance. The raking problem can be framed as minimization of a separable function subject to a simple equality constraint, with a corresponding dual computed using (13):

$$\mathcal{P} : \min_{\beta} \sum_i f_i(\beta_i; y_i) \quad \text{s.t.} \quad \mathbf{1}^T \beta = s \quad \Longleftrightarrow \quad \min_{\lambda} \lambda s + \sum_i f_i^*(-\lambda) \quad : \mathcal{D} \quad (16)$$

with optimal solution pair (β^*, λ^*) characterized by using 8:

$$\beta^* = \nabla_z f^*(-\lambda^* \mathbf{1}) \quad \text{or} \quad \beta_i^* = \nabla_z f_i^*(-\lambda^*). \quad (17)$$

²<https://pypi.org/project/raking/>

For the entropic distance function, we have

$$f_i(\beta_i, y_i) = \beta_i \ln \left(\frac{\beta_i}{y_i} \right) - (\beta_i - y_i) \iff f_i^*(z) = y_i (\exp(z) - 1), \quad (18)$$

and so (17) simplifies to

$$\beta^* = y \odot \exp(-\lambda \mathbf{1}) \quad \text{or} \quad \beta_i^* = y_i \exp(-\lambda) \quad (19)$$

By taking the derivative of the dual problem (16), we finally get

$$s = \sum_i y_i \exp(-\lambda) \Rightarrow \exp(-\lambda) = \frac{s}{\sum_i y_i}, \quad \beta^* = y \odot \exp(-\lambda \mathbf{1}) = \frac{s}{\sum_i y_i} y. \quad (20)$$

This computation recovers the classic bedrock result that 1D raking with entropic distance scales observations by the ratio of the constraint and sum.

2.2 2D Raking and IPF

Two-dimensional entropic raking no longer admits a closed form solution. Instead, we use the special structure of the 2D raking problem to understand the Iterative Proportional Fitting (IPF) algorithm from a dual perspective.

The general 2D raking problem with unknown $\beta \in \mathbb{R}^{m \times n}$ can be written as:

$$\begin{aligned} \mathcal{P} : \quad & \min_{\beta} f(\beta; Y) \quad \text{s.t.} \quad \beta \mathbf{1}_n = s_r, \quad \beta^T \mathbf{1}_m = s_c. \\ \mathcal{L} : \quad & f(\beta) + \lambda_r^T (\beta \mathbf{1}_n - s_r) + \lambda_c^T (\beta^T \mathbf{1}_m - s_c) \\ \mathcal{D} : \quad & \min_{\lambda_r, \lambda_c} \lambda_c^T s_c + \lambda_r^T s_r + \sum_{i,j} f_{ij}^*(-\lambda_r^i - \lambda_c^j) \\ \text{OPT} : \quad & \beta = \nabla_z f^*(-\lambda_r \otimes \lambda_c^T) \quad \text{or} \quad \beta_{ij} = \nabla_z f^*(-\lambda_r^i - \lambda_c^j). \end{aligned} \quad (21)$$

where f is separable, smooth, and has a smooth conjugate; the 2D structure is explicitly used to frame $\lambda_r \in \mathbb{R}^m$ and $\lambda_c \in \mathbb{R}^n$ as ‘row’ and ‘column’ multiplier vectors.

The IPF iteration and equivalent Sinkhorn algorithm take advantage of the fact that for entropic distance, we have

$$\nabla_z f_{ij}^*(-\lambda_r^i - \lambda_c^j) = y_{ij} \exp(-\lambda_r^i) \exp(-\lambda_c^j)$$

with two blocks λ_r and λ_c and dual objective that is separable with respect to one block when the other is fixed. Moreover, partial minimizers for each block are available in closed form, allowing a block-coordinate update:

$$\begin{aligned}\exp(-\lambda_r^i)^+ &= s_r^i / \sum_j y_{ij} \exp(-\lambda_c^j) \quad \text{for } i = 1, \dots, m \\ \exp(-\lambda_c^j)^+ &= s_c^j / \sum_i y_{ij} \exp(-\lambda_r^i)^+ \quad \text{for } j = 1, \dots, n.\end{aligned}$$

While IPF is typically viewed as iterative scaling for rows and columns of β to satisfy alternating sets of primal constraints, in light of (21) it is also an alternating maximization method for the dual. The updates are fully independent within each block, so they can be parallelized across the m rows and n columns. These key findings, together with the impressive performance of block coordinate descent, explain the emphasis of previous literature on IPF and Sinkhorn (Deming and Stephan (1940); Stephan (1942); She and Tang (2019); Cuturi (2013)).

For the two-dimensional raking case, we can make the Hessian-vector product structure more apparent. We first rewrite the row and column constraints as a single set of equality constraints $A\beta = \tilde{s}$. Define $\beta = \text{vec}(\beta)$ and recall the classic vec-kron identity

$$\text{vec}(ABC) = [C^T \otimes A] \text{vec}(B). \quad (22)$$

Using (22) we can directly write

$$\begin{aligned}\text{vec}(I_m \beta \mathbb{1}_m) &= (\mathbb{1}_n^T \otimes I_m) \beta \\ \text{vec}(\mathbb{1}_m^T \beta I_n) &= (I_n \otimes \mathbb{1}_m^T) \beta\end{aligned} \quad A = \begin{bmatrix} \mathbb{1}_n^T \otimes I_m \\ I_n \otimes \mathbb{1}_m^T \end{bmatrix}, \quad \tilde{s} = \begin{bmatrix} s_r \\ s_c \end{bmatrix}. \quad (23)$$

and the dual in (21) can be written as

$$\mathcal{D} : \min_{\lambda_c, \lambda_r} \lambda_c^T s_c + \lambda_r^T s_r + f^*(-(\mathbb{1}_n \otimes I_m) \lambda_r - (I_n \otimes \mathbb{1}_m) \lambda_c). \quad (24)$$

The Hessian of the dual objective is given by

$$H = ASA^T, \quad S = \nabla_z^2 f^*(-(\mathbb{1}_n \otimes I_m) \lambda_r - (I_n \otimes \mathbb{1}_m) \lambda_c)$$

where S is diagonal since f is separable across coordinates, and $A \in \mathbb{R}^{(n+m) \times (n+m)}$. The separability between row and column blocks is manifest in the structure of H :

$$ASA^T = \begin{bmatrix} \mathbb{1}_n^T \otimes I_m \\ I_n \otimes \mathbb{1}_m^T \end{bmatrix} S \begin{bmatrix} \mathbb{1}_n \otimes I_m & I_n \otimes \mathbb{1}_m \end{bmatrix} = \begin{pmatrix} [\mathbb{1}_n^T \otimes I_m] S [\mathbb{1}_n \otimes I_m] & [\mathbb{1}_n^T \otimes I_m] S [I_n \otimes \mathbb{1}_m] \\ [I_n \otimes \mathbb{1}_m^T] S [\mathbb{1}_n \otimes I_m] & [I_n \otimes \mathbb{1}_m^T] S [I_n \otimes \mathbb{1}_m] \end{pmatrix}.$$

The top left and bottom right blocks are diagonal:

$$(\mathbb{1}_n^T \otimes I_m) S (\mathbb{1}_n \otimes I_m) = \sum_{i=1}^n S_i, \quad [I_n \otimes \mathbb{1}_m^T] S [I_n \otimes \mathbb{1}_m] = \sum_{i=1}^m (PS)_i$$

where $S_i \in \mathbb{R}^{m \times m}$ are diagonal blocks of $S \in \mathbb{R}^{mn \times mn}$, and P is a permutation matrix that rearranges the order of the $n + m$ diagonal entries to follow row rather than column order, e.g. $P(\text{diag}(s_1, s_2, s_3, s_4, s_5, s_6)) = \text{diag}(s_1, s_4, s_2, s_5, s_3, s_6)$ for $m = 3, n = 2$. The IPF algorithm takes advantage of this explicit structure to implement block coordinate descent.

The key fact is that Hessian-vector products have $O(nm)$ complexity, just like IPF iterations:

$$ASA^T x = A \underbrace{\text{diag}(S) \odot (\text{vec}(x_{1:n} \mathbb{1}_m^T) + \text{vec}(\mathbb{1}_n x_{n+1:n+m}^T))}_z = \begin{bmatrix} Z \mathbb{1}_n \\ Z^T \mathbb{1}_m \end{bmatrix} \quad (25)$$

where $Z \in \mathbb{R}^{m \times n}$ is the vec adjoint (i.e. reshape) of $z \in \mathbb{R}^{nm \times 1}$.

While (25) gives insight into the 2D case, we do not need the specificity of (23) to get optimal $O(nm)$ complexity. All we need to know is that the number of nonzero entries in A for the 2D case is $O(nm)$, since in the classic case we have row and column constraints. Then it is immediate that applying A^T , scaling by S , and applying A are each $O(nm)$ operations. We compare the specialized IPF method for the 2D case to an inexact Newton method using the Minres subsolver in Figure 1. Inexact Newton works on the dual, and relies on problem structure only sparsity of A ; it is agnostic to the full specificity of (23). Nonetheless, it outperforms IPF both in dual gap and constraint violation.

As we generalize the raking framework, we favor the inexact Newton approach that seamlessly leverages sparsity of linear operators, and avoids the need for specialized IPF development for each innovation.

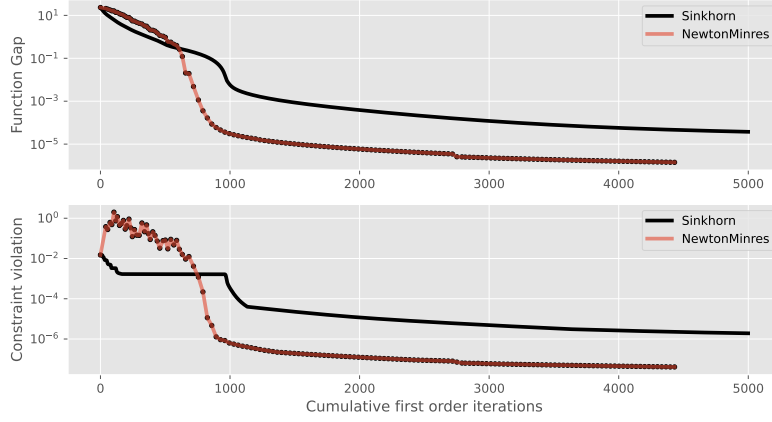


Figure 1: Sinkhorn/IPF iteration (black) vs. inexact Newton on the dual in terms of cumulative matrix vector products (x-axis). Top panel shows function gap on the dual objective, while bottom panel shows the maximum constraint violation. The Newton algorithm uses the iterative Minres subsolver, relying only on efficient Hessian-vector products, and solves to a relative tolerance of 10^{-4} with a maximum of 100 iterations. We set $n = 300$, $m = 200$, $s_r = \frac{1}{n} \mathbb{1}_n$, $s_c = \frac{1}{m} \mathbb{1}_m$, and $\log(y_{ij}) \stackrel{iid}{\sim} N(0, 200^2)$.

2.3 Raking in Higher Dimensions

The 2D case in Section 2.2 allows for a compact representation of the constraint matrix A (24). In higher dimensions, A can be viewed as a general sparse linear operator acting on the vector β that contains all estimates of interest. For example, considering the 3D case with dimensions m, n, p , we have $\beta \in \mathbb{R}^{mnp \times 1}$ and $A \in \mathbb{R}^{(mn+mp+np) \times mnp}$ is sparse, with $O(mnp)$ entries. In the general case, let $k = 1, \dots, d$ index dimension, and let m_k represent the cardinality of dimension k . Defining now

$$N := \prod_{k=1}^d m_k, \quad M := \sum_{k=1}^d N/m_k$$

we have $\beta \in \mathbb{R}^N$, and $A \in \mathbb{R}^{M \times N}$ with $O(dN)$ entries, since we have $O(N)$ in each dimension.

The number of dimensions d and cardinality within each dimension place inherent computational limits on general raking. However, the underlying problem is exactly as laid out

in Section 1.3.

$$\begin{aligned}
\mathcal{P} : \quad & \min_{\beta} f(\beta) \quad \text{s.t.} \quad A\beta = s \\
\mathcal{L} : \quad & f(\beta) + \lambda^T (A\beta - s) \\
\mathcal{D} : \quad & \min_{\lambda} f^*(-A^T \lambda) + \lambda^T s \\
\text{OPT} : \quad & \beta^* = \nabla_z f^*(-A^T \lambda^*).
\end{aligned} \tag{26}$$

The dual is unconstrained and has smaller dimension than the primal when e.g. $d < m_k$ for each k . In practice we have not seen use cases above $d = 3$ dimensions. However, the raking package we provide is dimension agnostic, and the user can enter any number of dimensions using the interface provided, as discussed in Section 3.1.

2.4 Raking with Different Losses

The entropic distance (18) appears to be a natural choice of raking objective given the 1D case (20). However, simpler functions have computational advantages, while more complex functions achieve additional aims, such as maintaining upper as well as lower bounds. In this section we present alternative raking losses and summarize all for convenience. All of the functions we use here are convex and differentiable, with differentiable conjugates; they also satisfy $f(y, y) = 0$.

Weighted Least Squares. We can compute the Taylor expansion of entropic distance (18) centered at $x = y$.

$$\begin{aligned}
f(\beta; y) &= \beta \log \left(\frac{\beta}{y} \right) - (\beta - y) & \Rightarrow & \quad f(y, y) = 0 \\
f'(\beta; y) &= \log \left(\frac{\beta}{y} \right) & \Rightarrow & \quad f'(y, y) = 0 \\
f''(\beta; y) &= \frac{1}{\beta} & \Rightarrow & \quad f''(y, y) = \frac{1}{y}
\end{aligned}$$

Thus the second order Taylor expansion of the entropic distance function gives rise to a weighted least squares, or χ -square:

$$\beta \log \left(\frac{\beta}{y} \right) - (\beta - y) \approx \frac{1}{2y} (\beta - y)^2 := f_2(\beta; y).$$

The function $\frac{1}{2}|\beta|^2$ is self-conjugate, so using (9) we have

$$f_2^*(z) = y \left(\frac{z^2}{2} + z \right) \quad \text{and} \quad \nabla_z f_2^*(z) = y(z + 1).$$

Since f_2 is a quadratic, the dual problem (26) has closed form solution:

$$\begin{aligned} \min_{\lambda} \left\{ \frac{1}{2} \lambda^T A Y A^T \lambda - \lambda^T (A y - s) \right\} \\ A y - s = A Y A^T \lambda \quad \Rightarrow \quad \lambda^* = (A Y A^T)^{-1} (A y - s). \\ \beta^* = \nabla_z f^*(-A^T \lambda^*) = y \odot \left(1 - A^T (A Y A^T)^{-1} (A y - s) \right). \end{aligned}$$

By construction, β^* in (26) is always primal feasible. In this case, the reader can check explicitly that $A\beta^* = s$. The closed form rake is convenient, but the output is not guaranteed to be positive when the input is positive.

Entropic Loss. From Section 2.1, we have

$$f_i(\beta_i, y_i) = \beta_i \log \left(\frac{\beta_i}{y_i} \right) - (\beta_i - y_i) \quad \Longleftrightarrow \quad f_i^*(z) = y_i (\exp(z) - 1),$$

and thus OPT in (26) gives

$$\beta^* = y \odot \exp(-A^T \lambda^*).$$

The dual solution outside of the 1D case does not admit a closed form, but the primal-dual relationship makes it clear that the raked values are obtained by differential scaling, and outputs are positive when the inputs are positive, and zero when inputs are zero.

Logistic Loss. A common use case for raking is that of bounded quantities, where we have upper bounds on each value raked in addition to aggregation constraints. We can seamlessly add bound constraints by adopting a logistic loss with domain $l \leq \beta \leq u$.

$$f_i(\beta_i, y_i) = (\beta_i - l_i) \log \left(\frac{\beta_i - l_i}{y_i - l_i} \right) + (u_i - \beta_i) \log \left(\frac{u_i - \beta_i}{u_i - y_i} \right)$$

The computation of the final conjugate is detailed in Appendix A.2. We have

$$f^*(z) = (u - l) \log \left(\frac{y - l}{u - l} \exp(z) + \frac{u - y}{u - l} \right) + lz.$$

The OPT condition in (26) gives

$$\beta^* = l + (u - l) \odot \left(\frac{(y - l) \odot \exp(-A^T \lambda^*)}{(y - l) \odot \exp(-A^T \lambda^*) + u - y} \right)$$

which the reader can verify satisfies the bound constraint $l \leq \beta \leq u$ whenever y satisfies the same constraint. The logistic loss thus enforces the bounds while preserving the simple problem structure of (26).

We show in Appendix B.1 how the choice of the raking loss affects the final raked values.

2.5 Raking with Differential Weights

In many use cases, inputs y_i are modeled quantities that come with uncertainty information. Introducing weights allows us to account for these uncertainties so that more certain inputs move less during the raking process compared to less certain inputs. For example, a simple approach to re-weighting is to take the weights w_i equal to $\frac{1}{\sigma_i^2}$ where σ_i is the standard deviation of the reported y_i .

The special case of 1D raking is detailed in Appendix A.1. For the general case, the duality framework (26) seamlessly accommodates differential weights. Define

$$f^w(\beta) = \sum_i w_i f_i(\beta).$$

Then we have

$$(f_i^{w_i})^*(\beta_i) = w_i f_i^*\left(\frac{\beta_i}{w_i}\right), \quad \beta^* = \nabla_z f^* \left(- (A^T \lambda^*) \odot \frac{1}{w} \right).$$

As any weight w_i goes to infinity, the corresponding solution β_i^* goes to $\nabla_z f_i^*(0)$. By (8), this is equivalent to $0 = \nabla_{\beta} f_i(\beta_i^*)$ and occurs if and only if $\beta_i = y_i$.

We illustrate in Appendix B.2 how raking with weights and using the known aggregate allows retrieving the true value of a biased observation.

2.6 Raking with Aggregate Observations

While in some cases it is natural to frame aggregates as constraints, in other contexts aggregates may themselves be noisy or uncertain. Williams and Savitsky (2024) used losses applied to aggregates rather than treating all aggregates as constraints to deal with inconsistent observations. In the context of global health, some information must be treated as constraints, while other information is more naturally classified as observations.

The natural extension of (26) is to separate the loss into two components:

$$\min_{\beta} f_1(\beta) + f_2(B\beta) \quad \text{s.t.} \quad A\beta = s. \quad (27)$$

This is in fact exactly the strategy of Williams and Savitsky (2024). Here we provide an explicit dual structure that informs our approach.

We define an auxiliary and introduce an additional constraint $\zeta := B\beta$. Considering the combined block of variables $[\beta^T, \zeta^T]^T$ together with the expanded constraint set (28) immediately lets us compute the dual to (27) using (14) and (15):

$$\begin{aligned} \mathcal{P} : \quad & \min_{\beta, \zeta} f_1(\beta) + f_2(\zeta) \quad \text{s.t.} \quad \begin{bmatrix} A & 0 \\ B & -I \end{bmatrix} \begin{bmatrix} \beta \\ \zeta \end{bmatrix} = \begin{bmatrix} s \\ 0 \end{bmatrix} \\ \mathcal{L} : \quad & f_1(\beta) + f_2(\zeta) + \lambda_1^T (A\beta - s) + \lambda_2^T (B\beta - \zeta) \\ \mathcal{D} : \quad & \min_{\lambda_1, \lambda_2} \lambda_1^T s + f_2^*(\lambda_2) + f_1^*(-A^T \lambda_1 - B^T \lambda_2). \\ \text{OPT} \quad & \zeta^* = \nabla_z f_2^*(\lambda_2^*), \quad \beta^* = \nabla_z f_1^*(-A^T \lambda_1^* - B^T \lambda_2^*) \end{aligned} \quad (28)$$

The system (28) is very interesting. It tells us that from the point of view of the optimization problem it makes very little difference whether we treat aggregates as constraints (that is, add rows to A) or as observations (that is, add rows to B). No matter what we do with any particular aggregate, we end up with a dual problem whose dimension is equal to the sum of the different inputs, whether they are treated as constraints or as observations. This fully preserves the efficient computational structure discussed in the previous section.

Consider the curious extreme where we treat all aggregates s as observations rather than constraints. In this case, the affine term $\lambda_1^T s$ and constraint matrix A would not be used, but we would have $B = A$, and the dual we are left with is

$$\min_{\lambda} f_2^*(\lambda) + f_1^*(-A^T \lambda).$$

where we renamed λ_2 to λ to highlight the similarity to (26). If we use entropic distance for f_2 , we would have

$$f_2^*(\lambda) = s \odot (\exp(\lambda) - 1) \approx \lambda^T s$$

where the approximation above is linear. So the difference between the extremes of treating all aggregates as constraints or observations is whether we use an affine term or a closely related exponential term in the dual. Having solved the dual, the primal-dual recovery equation is identical:

$$\beta^* = \nabla_z f_1^*(-A^T \lambda^*).$$

We provide a simple interface to the user to declare whether an aggregate is a constraint or observation by using a ‘weights’ column, where an infinite entry indicates a constraint, and a finite entry an observation weight.

We illustrate the impact of using a weighted aggregate instead of a constraint on a simple example in Appendix B.3.

2.7 Raking with Missing Data

Here we develop a duality-based approach for raking with missing observations.

Consider a 2×2 array with three missing observations:

$$y = \begin{bmatrix} 2.0 & \text{NA} \\ \text{NA} & \text{NA} \end{bmatrix}$$

The missing entries can be inferred given a constraint on the first row and column, and one additional constraint on the second row or second column. For example, if the first row is

constrained to sum to 3, then the top right entry will be set to 1, while if it is constrained to sum to 1, then the entry will be set to 0 while the original observation would be adjusted to 1.0. Conversely, if we are missing any of the three pieces of information described above, we cannot infer the entire array.

To model the missing entries, consider the matrix P to be a permutation matrix that selects the $\tilde{p} \leq p$ entries of β that have observations, so $PP^T = I_{\tilde{p}}$, while $P^TP \in \mathbb{R}^{p \times p}$ is the projector onto the space of observations, that is, it acts as the identity on observed coordinates and 0 on the unobserved. Analogously, $I - P^TP$ is the projector onto the complement space of entries that are not observed. The structure of the problem with missing data and aggregate observations is:

$$\mathcal{P} : \min_{\beta} f_1(P\beta) + f_2(B\beta) \quad \text{s.t.} \quad A\beta = s.$$

We also define $\zeta = P\beta + B\beta$ and a combined matrix to model the selection and aggregation, and the corresponding dual variables:

$$D = \begin{bmatrix} P \\ B \end{bmatrix}, \quad \lambda_D = \begin{bmatrix} \lambda_P \\ \lambda_B \end{bmatrix}.$$

Our overall problem now has the following structure:

$$\begin{aligned} \mathcal{P} : \quad & \min_{\beta, \zeta} f(\zeta) \quad \text{s.t.} \quad \begin{bmatrix} A & 0 \\ D & -I \end{bmatrix} \begin{bmatrix} \beta \\ \zeta \end{bmatrix} = \begin{bmatrix} s \\ 0 \end{bmatrix} \\ \mathcal{L} : \quad & f(\zeta) + \lambda_A^T (A\beta - s) + \lambda_D^T (D\beta - \zeta) \\ \mathcal{D} : \quad & \min_{\lambda_A, \lambda_D} \lambda_A^T s + f^*(\lambda_D) + \delta_0(-A^T \lambda_A - D^T \lambda_D). \\ \text{OPT} : \quad & \zeta^* = \nabla_z f^*(\lambda_D^*), \quad \begin{bmatrix} A \\ D \end{bmatrix} \beta^* = \begin{bmatrix} s \\ \zeta^* \end{bmatrix} \end{aligned} \tag{29}$$

Here the problem has both a larger dual dimension and additional affine constraints compared to (28). However, there is more structure that we can exploit within the affine

constraint in \mathcal{D} and we can reduce the problem dimension and complexity. The dual affine constraint in (29) can be used to solve for λ_P :

$$\lambda_P = -P (A^T \lambda_A + B^T \lambda_B).$$

Plugging the solution back into the constraint we get

$$0 = A^T \lambda_A - P^T P (A^T \lambda_A + B^T \lambda_B) + B^T \lambda_B = (I - P^T P) (A^T \lambda_A + B^T \lambda_B).$$

The reduced dual problem is given by

$$\begin{aligned} \mathcal{D}_r : \quad & \min_{\lambda_A, \lambda_B} \lambda_A^T s + f^* \left(\begin{bmatrix} -PA^T & -PB^T \\ 0 & I \end{bmatrix} \begin{bmatrix} \lambda_A \\ \lambda_B \end{bmatrix} \right) \\ \text{s.t.} \quad & (I - P^T P) (A^T \lambda_A + B^T \lambda_B) = 0. \end{aligned} \tag{30}$$

The new dual affine constraint is exactly informed by the unobserved coordinates, since $I - P^T P$ projects onto these. The problem thus has the same dimension as (28), and as many constraints as missing observations. We can easily apply Newton's method, particularly since it guarantees affine constraints are satisfied at each iteration.

To recover β^* , we first recall that from the optimality conditions (29),

$$\begin{aligned} \zeta^* &= \nabla_z f^* (\lambda_D^*) = \nabla_z f^* \begin{pmatrix} -P (A^T \lambda_A^* + B^T \lambda_B^*) \\ \lambda_B^* \end{pmatrix} \\ P\beta^* &= \nabla_z f^* (-P (A^T \lambda_A + B^T \lambda_B)) \end{aligned}$$

which means we can read off the solutions corresponding to those entries that were observed directly from evaluating the first component of the gradient of the dual objective in (30). This means we can rake observed values regardless of the missingness pattern.

All that remains are the unobserved entries of β , which are precisely the Lagrange multipliers for the affine constraint of the reduced dual (30). Optimality of the associated Lagrangian with respect to λ as in (15) yields

$$\begin{bmatrix} A \\ B \end{bmatrix} (I - P^T P) \beta^* = - \begin{bmatrix} s \\ 0 \end{bmatrix} - \begin{bmatrix} -AP^T & 0 \\ -BP^T & I \end{bmatrix} \nabla_z f^* \left(\begin{bmatrix} -PA^T & -PB^T \\ 0 & I \end{bmatrix} \begin{bmatrix} \lambda_A^* \\ \lambda_B^* \end{bmatrix} \right).$$

Thus we can rake missing observations exactly when the columns of the stack of A and B corresponding to unobserved coordinates of β has full rank.

We show in Appendix B.4 how the raking of available observations and known aggregates allows imputing missing values while respecting constraints.

2.8 Uncertainty Quantification

Computing the variance of the estimator (1) is important for all variants of raking problems. In the survey flavor of raking, the quantities $y_i, i \in S$ are known and so the variance of the estimator is informed by the selection of the sample S from the population \mathcal{U} and uncertainty on the marginal totals $\sum_{i \in \mathcal{U}} x_i$. The variance of the estimator (1) proposed by Narain (1951); Horvitz and Thompson (1952) is

$$\mathbb{V}(\hat{\mathcal{Y}}) = \sum_{k,l \in \mathcal{U}} (\pi_{kl} - \pi_k \pi_l) \frac{y_k}{\pi_k} \frac{y_l}{\pi_l}. \quad (31)$$

Lu and Gelman (2003) used the uncertainty on the raking weights to compute the variance of the resulting estimate. Kim et al. (2011) accounted for the raking procedure to estimate the variance of the estimator. Moretti and Whitworth (2023) used bootstrap method to estimate the uncertainty of the raking estimator for small area estimation. A review on methods to use priors on the margins to compute the posterior distribution for the total \mathcal{Y} is given in Si and Zhou (2021).

The focus of raking in global health is different. Here, sum \mathcal{Y} and its variance are known, and we are interested in using the known variances and covariances on the observations y and the margins s to estimate the unknown covariance matrix of the raked values β . In our typical use case, we rectify detailed estimates with aggregated estimates from different models, and seek to propagate uncertainty to obtain the correct variance of the adjusted estimates.

The technical challenge for variance estimation in the global health context is that uncertainty is present in both the initial estimates and the constraints. To incorporate the

idea of *uncertain constraints* we consider that the ‘mean constraint’ must hold for the final estimate, but uncertainty in the right-hand side (that is, the variance of the aggregates) should rigorously inform the variance of the final estimator.

The particular case where the raked values can be written as a linear combination of y and s is detailed in Appendix A.3. In the general case, we use the implicit function theorem to get a generalized delta method for uncertainty propagation. In particular, we define

$$F(\beta^*, \lambda^*; y, s) := \nabla \mathcal{L}(\beta^*, \lambda^*) = \begin{bmatrix} W \nabla_{\beta} f(\beta^*; y) + A^T \lambda^* \\ A\beta^* - s \end{bmatrix} = 0. \quad (32)$$

The solution of this system can be written as

$$\beta^* = \phi(y; s) \text{ with } \phi : \mathbb{R}^{p+k} \rightarrow \mathbb{R}^p. \quad (33)$$

Theorem 1: Covariance of the Raked Values Suppose that the vector of observations and margins (y, s) is a random vector with expectation θ and covariance matrix Σ . Given n samples, denoted $(y^{(i)}, s^{(i)})$ for $i = 1, \dots, n$, denote their sample mean by (\bar{y}_n, \bar{s}_n) . Let ϕ'_{θ} denote the matrix of the partial derivatives of ϕ with respect to the observations y and margins s taken at θ . If β_n^* denotes the raked values of the sample mean, then the covariance matrix of the raked values β_n^* is given by

$$\Sigma_{\beta_n} = \phi'_{\theta} \Sigma \phi_{\theta}'^T.$$

The proof is given in Appendix A.4. Theorem 1 extends the delta method to the higher dimensional setting, where in addition to the classic p scoring equations we have k additional equations with randomly distributed right hand sides to inform the estimate.

In current practice, scientists often use samples of original estimates and the margins, called *draws*, to estimate the variance of the raked estimates. In this scheme, the raking problem is solved for each draw of observations and margins, and then the mean and variance are computed from the outputs.

To understand this process better, consider the raked values of the random vector (y, s) , by denoted $\phi(y, s)$ with expectation $\mathbb{E}\phi$ and covariance matrix Σ_β . Given n samples of the raked vector $\phi(y^{(i)}, s^{(i)})$, from the central limit theorem we have

$$\sqrt{n} \left(\frac{1}{n} \sum_{i=0}^n \phi \begin{pmatrix} y^{(i)} \\ s^{(i)} \end{pmatrix} - \mathbb{E}\phi \begin{pmatrix} y \\ s \end{pmatrix} \right) \rightarrow \mathcal{N}(0, \Sigma_\beta). \quad (34)$$

If to first order we have

$$\frac{1}{n} \sum_{i=0}^n \phi \begin{pmatrix} y^{(i)} \\ s^{(i)} \end{pmatrix} \approx \phi \begin{pmatrix} \bar{y}_n \\ \bar{s}_n \end{pmatrix}, \quad (35)$$

then from Theorem 1 and (34) the draws process has the asymptotically correct statistics

$$\mathbb{E}\phi \begin{pmatrix} y \\ s \end{pmatrix} \approx \phi(\theta) \text{ and } \Sigma_\beta \approx \phi'_\theta \Sigma \phi'^T_\theta. \quad (36)$$

The approximation (35) is an equality when ϕ is a linear map, for example, in linear regression. When ϕ is nonlinear, or affine constraints are present, (35) may not hold. For the raking problem, we show empirically in the experiments that given enough draws we actually can get close to the asymptotic statistics, but we incur a systematic bias when we use the draws.

To compute Σ_β in the general case, we now need to compute the partial derivatives $\frac{\partial \phi_j}{\partial y_i}$ and $\frac{\partial \phi_j}{\partial s_i}$. We use the Implicit Function Theorem (IFT) Folland (2002), adapted to our case in Appendix A.5.

3 Verifications

3.1 User Interface

Here we describe the simple user interface used to implement different flavors of raking detailed in Section 2. The observations and margins are given by the user through a Pandas data frame containing the following columns:

- ‘value’ column: Value of an observation, a constraint, or ‘NaN’ if missing.
- ‘weight’: Positive value for an observation, 0 for missing, or ‘inf’ for constraint.
- Categorical values of dimension columns (see below).

The user builds the data by providing the list of categorical variables and values corresponding to aggregates over given dimension, and names for value and weight columns. For a table 2×2 with one missing value, the interface thus has the structure given in Table 1. The user then needs to specify the data builder:

Table 1: Full 2D problem specification. The first four entries specify granular observations, with the NaN value and 0 weight in the fourth row indicating that the (2, 2) entry is missing. The last three rows specify aggregates using the special value 0 (see Data Builder below). Weights of ‘inf’ indicate that the first two aggregates are set as constraints; while the last row specifies an observation-type aggregate.

| value | X1 | X2 | weights |
|-------|----|----|---------|
| 1.0 | 1 | 1 | 1.0 |
| 2.0 | 1 | 2 | 1.0 |
| 3.0 | 2 | 1 | 1.0 |
| NaN | 2 | 2 | 0.0 |
| 4.0 | 1 | 0 | inf |
| 7.0 | 2 | 0 | inf |
| 5.0 | 0 | 1 | 10 |

```
data_builder = DataBuilder(
    dim_specs={'X1': 0, 'X2': 0},
    value='value',
```

```
weights='weights')
```

For mortality estimates in Section 3.3, a partial specification is shown in Table 2 and the data builder is defined as below:

```
data_builder = DataBuilder(  
    dim_specs={'cause': 0, 'race': 0, 'county': 0},  
    value='value',  
    weights='weights',
```

Table 2: Select rows from specification of the Mortality Application in Section 3.3, showing different levels of aggregates as well as margins and observations.

| | value | county | race | cause | weights |
|-----------|-------|--------|------|-------|---------|
| y_{001} | | 1 | 0 | 0 | 1.0 |
| y_{101} | | 1 | 0 | 1 | 1.0 |
| y_{0J1} | | 1 | J | 0 | 1.0 |
| y_{IJK} | | K | J | I | 1.0 |
| s_1 | | 0 | 0 | 1 | inf |

3.2 Verifications for Simple Cases

We apply the methods described in Section 2 to simple synthetic datasets. The impact of the raking loss is illustrated in Appendix B.1, the effect of raking with weights is illustrated in Appendix B.2, the use of aggregates as observations rather than constraints is illustrated in Appendix B.3, the strategies for missing data are illustrated in Appendix B.4, the effectiveness of the uncertainty quantification method is demonstrated in Appendix B.5.

3.3 Application to Mortality Estimates

The problem of reconciling detailed estimates (by county, race, and cause) with GBD estimates problem has been carefully considered within IHME, described in detail in Appendix C.1.

The data set (Dwyer-Lindgren et al. (2023)) contains the estimated number of deaths by cause, race / ethnicity, and county for each US state, year, sex and age group. These estimates are raked to aggregate estimates, typically all-race state-wide cause-specific and all-cause counts, while trying to preserve key relational information in the detailed estimates, as described below and summarized in Figure 2.

There are $I = 3$ different causes: communicable, maternal, neonatal, and nutritional diseases (Comm.), non-communicable diseases (NCD), and injuries (Inj.) and $J = 5$ different race / ethnicity groups: White, Black, American Indian or Alaska Native (AIAN), Asian or Pacific Islander (API), and Hispanic/Latino (Hisp.). We denote $y_{i,j,k}$ the number of deaths for cause $i = 1, \dots, I$, race $j = 1, \dots, J$ and county $k = 1, \dots, K$. We use $i = 0$ for the sum of deaths over all causes, $j = 0$ for the sum of deaths over all races, and $k = 0$ for the sum of deaths over all counties, i.e. the number of deaths at the state level. Aggregate data are provided by the GBD (Causes of Death Collaborators (2018)) and are the total number of deaths for the state $s_0 = y_{0,0,0}$ and the number of deaths due to cause i for the state $s_i = y_{i,0,0}$. The margins must be used as constraints, so $s_0 = \sum_{i=1}^I s_i$ (shown as teal blocks in Figure 2). On the other hand, all-cause aggregates by race and county, all-cause all-race aggregates by county, and all-race cause-specific aggregates by county may not be consistent and can be used as observations (shown as gray blocks in Figure 2).

Denoting β the length- IJK vector containing the unknown raked values for each cause i , each race j and each county k , and s the length- I vector containing the number of deaths due to each cause i for the state, we can rewrite the problem under the form 27 in Section 2.6, where B encodes the aggregation observations, while A encodes the aggregation

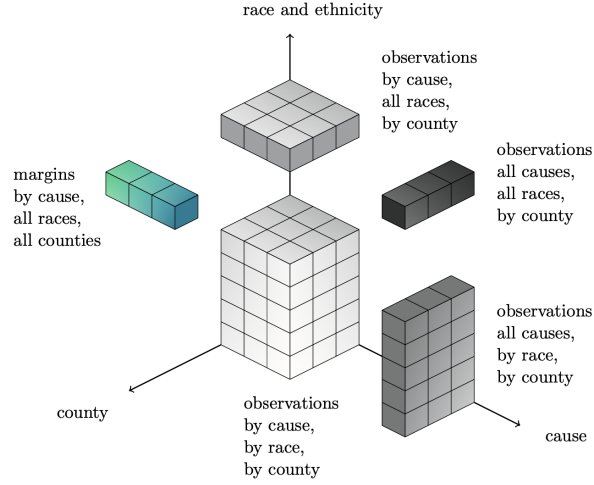


Figure 2: Summary of the raking problem for the mortality estimates dataset.

constraints.

We compare the raked values with their associated uncertainty to the initial values. To better compare the different causes, races and counties on the same scale, we compare mortality rates. In Figure 3, we look at the initial values and the raked values for both-sex Delaware, age group 25-to-30-year-old. The uncertainty is represented by a segment of length two standard deviations and centered on the estimated value. Races AIAN and API with much smaller population numbers have the largest uncertainties for both the initial and the raked values. This uncertainty on the raked values is significantly reduced compared to the uncertainty on the initial values. The initial uncertainty on the margins s (that is on the GBD values) are smaller than the uncertainties on the observations y , and as a result the raking process significantly decreases the final uncertainty on these raked values.

To estimate how the initial values influence the raked values, we look at the initial value for cause “injuries” (Inj), race group White and New Castle County (denoted $y_{2,1,2}$). Then we compute the corresponding values of the gradient $\frac{\partial \beta_{i,j,k}}{\partial y_{2,1,2}}$ for $i = 0, \dots, 3$, $j = 0, \dots, 5$ and $k = 1, 2, 3$. The corresponding values of the gradient are shown in Figure 4. The

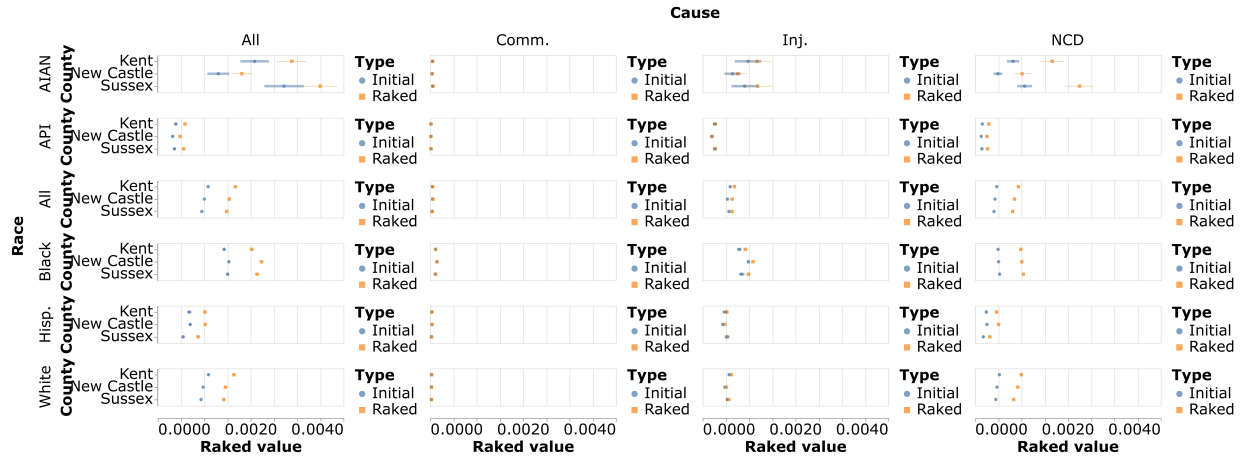


Figure 3: Initial and raked values with associated uncertainty ordered by county. The raked values are close to the initial observations, but have smaller uncertainties as the uncertainty on the margins is smaller than the uncertainty reported for the observations. The corresponding figures with initial and raked values ordered by cause and race are provided in Appendix C.2.

most affected raked value is the one with the same cause, race and county as the initial value considered. All causes deaths for race group White and New Castle County and all races deaths for cause “injuries” and New Castle County will be positively influenced by variations in the initial value $y_{2,1,2}$ while other causes and races will be negatively influenced. The raked values in the other counties will not be much affected by changes in the value of $y_{2,1,2}$. The converse result, which observation have the most influence on the final raked values, is presented in Appendix C.3.

Finally, we compute the variance of the estimated raked values using two methods: First, we take 100 samples of the detailed and aggregate observations, apply the raking procedure to each sample, and compute the sample mean and the sample variance of the corresponding raked values. Second, we compute the sample mean of the initial data set, apply the raking procedure to the sample mean, and use the delta method and the implicit function theorem to propagate the variance of the observations to get the variance of the

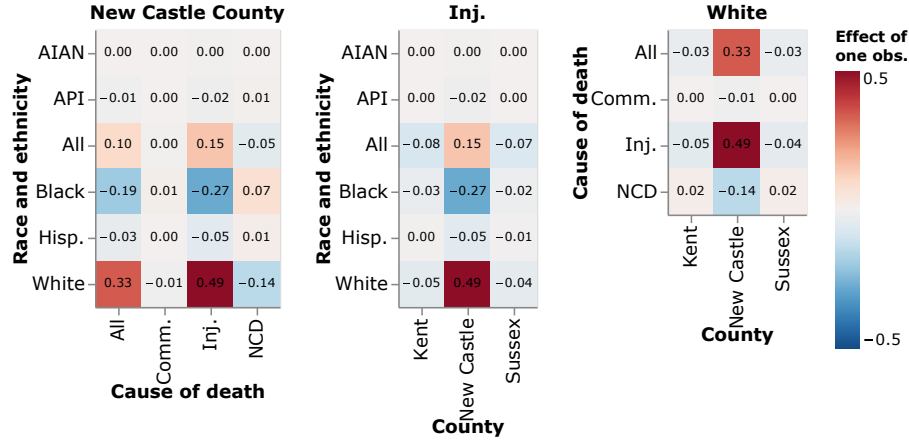


Figure 4: Influence of the initial value of deaths for cause injuries, race group White and New Castle County on all the raked values. As expected, the corresponding raked value $\beta_{2,1,2}^*$ is the most affected, followed by the raked values for the partial totals $\beta_{0,1,2}^*$ and the $\beta_{2,0,2}^*$.

raked values. In Figure 5, we look at the raked values for Delaware, both-sexes, and age group 25-to-30-year-old and compare the raked values and their standard deviation computed with both methods. We see evidence of sampling variation in the draws method, which makes sense since we only have 100 draws. The results obtained with the delta method are therefore both more accurate and far more efficient to compute compared to a Monte Carlo technique that rakes all draws.

4 Conclusion

In this paper, we have reviewed the convex optimization foundation of raking, and focused on a dual perspective that simplifies and streamlines prior raking extensions and provides new functionality, enabling a unified approach to n -dimensional raking, raking with differential weights, ensuring bounds on estimates, raking to margins either as hard constraints or as aggregate observations, handling missing data, and allowing efficient uncertainty prop-

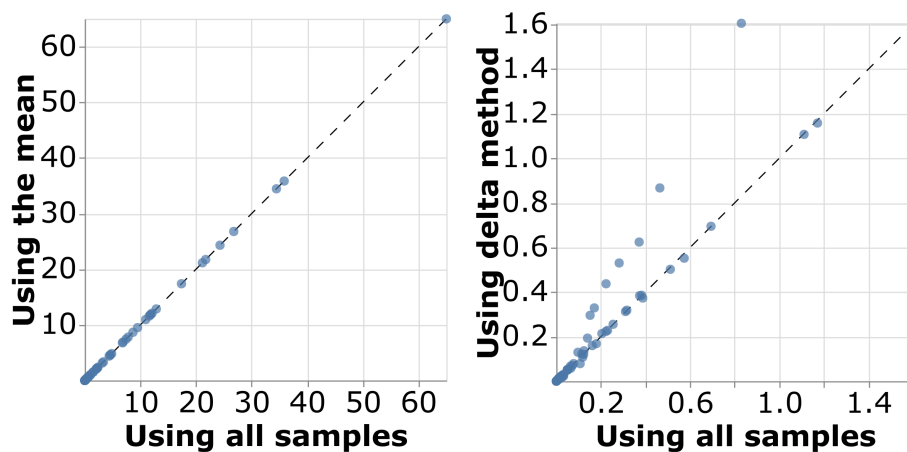


Figure 5: Comparison between the means (left) and the standard deviations (right) of the raked values computed with the delta method vs. 100 draws. The new delta method gives more accurate results than using limited draws.

agation. The dual perspective also enables a fast and scalable matrix-free optimization approach for all of these extensions. We illustrated the capabilities using synthetic data and real mortality estimates.

Acknowledgments

This work was funded by the Bill and Melinda Gates Foundation. An accompanying Python package can be found and installed through PyPI (<https://pypi.org/project/raking/>). It is also available on GitHub (<https://github.com/ihmeuw-msca/raking>). The Python scripts used to make the figures can be found on the Github account of the first author (<https://github.com/ADuce>).

A Technical Details and Proofs

A.1 1-D Raking with Weights

In this section we study the effect of non-uniform weights in Section 2.5 and aggregate data in Section 2.6 for the raking in the simple 1-dimensional case. If we scale losses f_i by observation-specific weights w_i , aggregating using non-uniform weights a_i , or do both within the same formulation, the closed form solution (20) is replaced by a nonlinear equation:

$$\min_{\lambda} \lambda s + \sum_i w_i f_i^* (-a_i \lambda / w_i) \iff s = \sum_i a_i (f_i^*)^{(1)} (-a_i \lambda / w_i) \quad (37)$$

where we used (9) to compute $(w_i f_i)^* (-a_i \lambda) = w_i f_i^* (-a_i \lambda / w_i)$ in the above. We can use Newton's method to solve (37):

$$\lambda^+ = \lambda - \tau \frac{s - \sum_i a_i (f_i^*)^{(1)} (-a_i \lambda / w_i)}{\sum_i \frac{a_i^2}{w_i} (f_i^*)^{(2)} (-a_i \lambda / w_i)}$$

with τ selected using a line search for the dual objective. Given dual solution λ^* , the primal β^* is given by

$$\beta_i^* = (f_i^*)^{(1)} (- (a_i / w_i) \lambda^*).$$

The key observation here is that, as we require more of the raking framework, some convenient idiosyncrasies (such as (20)) disappear, but the computational advantages of the dual remain: here, minimizing a scalar convex function is basically as easy as evaluating a closed form solution.

A.2 Conjugate of Logistic Loss

In this part, we detail the computation of the conjugate of the logistic loss given in Section 2.4. To compute the conjugate, we drop the index for convenience and define

$$\tilde{\beta} = \frac{\beta - l}{u - l}, \quad \tilde{y} = \frac{y - l}{u - l}, \quad f(\beta \mid y) = (u - l) \left(\tilde{\beta} \log \left(\frac{\tilde{\beta}}{\tilde{y}} \right) + (1 - \tilde{\beta}) \log \left(\frac{1 - \tilde{\beta}}{1 - \tilde{y}} \right) \right). \quad (38)$$

Next, we compute the conjugate of

$$\tilde{f}(x) = x \log\left(\frac{x}{y}\right) + (1-x) \log\left(\frac{1-x}{1-y}\right).$$

We have

$$\tilde{f}^*(z) = \sup_x \left[xz - x \log\left(\frac{x}{y}\right) - (1-x) \log\left(\frac{1-x}{1-y}\right) \right].$$

Taking the derivative with respect to x , we get

$$z = \log\left(\frac{x}{y}\right) - \log\left(\frac{1-x}{1-y}\right),$$

which gives us

$$\begin{aligned} \tilde{f}^*(z) &= x \left(\log\left(\frac{x(z)}{y}\right) - \log\left(\frac{1-x(z)}{1-y}\right) \right) - x(z) \log\left(\frac{x(z)}{y}\right) - (1-x(z)) \log\left(\frac{1-x(z)}{1-y}\right) \\ &= -\log\left(\frac{1-x(z)}{1-y}\right) = z - \log\left(\frac{x(z)}{y}\right), \quad x(z) = \frac{y}{y + (1-y) \exp(-z)}. \end{aligned}$$

Thus, we have

$$\tilde{f}^*(z) = z + \log(y + (1-y) \exp(-z)) = \log(y \exp(z) + (1-y)).$$

and the final conjugate is

$$\begin{aligned} f^*(z) &= (u-l) \log(\tilde{y} \exp(z) + (1-\tilde{y})) + lz \\ &= (u-l) \log\left(\frac{y-l}{u-l} \exp(z) + \frac{u-y}{u-l}\right) + lz. \end{aligned}$$

A.3 Uncertainty Quantification for the Least-Square Loss

In this section, we consider the least squares version of the raking problem, taking the loss to be $f(\beta_i, y_i) = \frac{w_i}{2} (\beta_i - y_i)^2$. We get the closed form solution

$$\lambda^* = \Phi^{-1}(Ay - s) \text{ and } \beta^* = (I - W^{-1}A^T\Phi^{-1}A)y + W^{-1}A^T\Phi^{-1}s, \quad (39)$$

where $W = \text{diag}(w)$ and $\Phi = AW^{-1}A^T$. Supposing that

$$V \left(\begin{bmatrix} y \\ s \end{bmatrix} \right) = \begin{bmatrix} \Sigma_y & \Sigma_{ys} \\ \Sigma_{ys}^T & \Sigma_s \end{bmatrix},$$

we can compute the variance of β^* explicitly using (39):

$$\begin{aligned} \Sigma_{\beta^*} &= (I - W^{-1}A^T\Phi^{-1}A) \Sigma_y (I - W^{-1}A^T\Phi^{-1}A)^T \\ &\quad + (W^{-1}A^T\Phi^{-1}) \Sigma_s (W^{-1}A^T\Phi^{-1})^T + 2 (I - W^{-1}A^T\Phi^{-1}A) \Sigma_{ys} (W^{-1}A^T\Phi^{-1})^T. \end{aligned} \quad (40)$$

The variance of the right hand side s , as well as the covariance of aggregates and observations is thus be propagated to inform the variance of the estimate, while the estimate itself satisfies the mean value of the constraint.

A.4 Proof of Theorem 1

Here, we detail the proof of Theorem 1, given in Section 2.8. From the central limit theorem, we have

$$\sqrt{n} \left(\begin{pmatrix} \bar{y}_n \\ \bar{s}_n \end{pmatrix} - \theta \right) \rightarrow \mathcal{N}(0, \Sigma), \quad \text{where} \quad \theta = \mathbb{E} \begin{pmatrix} y^{(i)} \\ s^{(i)} \end{pmatrix}, \quad \Sigma = \begin{pmatrix} \Sigma_y & \Sigma_{ys} \\ \Sigma_{ys} & \Sigma_s \end{pmatrix}. \quad (41)$$

If the mapping $\phi : \mathbb{R}^{p+k} \rightarrow \mathbb{R}^p$ from detailed and aggregate observations to the raked estimates is differentiable at θ , then we have that $\sqrt{n} \left(\phi \begin{pmatrix} \bar{y}_n \\ \bar{s}_n \end{pmatrix} - \phi(\theta) \right)$ converges weakly to a multivariate normal distribution with mean 0 and covariance $\phi'_\theta \Sigma \phi_\theta'^T$.

A.5 Implicit Function Theorem and Derivative Computations

We adapt the statement of the Implicit Function Theorem from Folland (2002). Assume that S is an open subset of \mathbb{R}^{2p+2k} and that $F : S \rightarrow \mathbb{R}^{p+k}$ is a function of class C^1 . Assume also that $(\beta^*, \lambda^*; y_0, s_0)$ is a point in S such that

$$F(\beta^*, \lambda^*; y_0, s_0) = 0, \quad \det D_{\beta, \lambda} F(\beta^*, \lambda^*; y_0, s_0) \neq 0 \quad (42)$$

where $D_{\beta, \lambda} F$ is the matrix of partial derivatives. We have the following:

- i. There exist $r_0, r_1 > 0$ such that for every $(y, s) \in \mathbb{R}^{p+k}$ with

$$\|(y, s) - (y_0, s_0)\| < r_0,$$

there is a unique $(\beta, \lambda) \in \mathbb{R}^{p+k}$ such that

$$\|(\beta, \lambda) - (\beta^*, \lambda^*)\| < r_1 \text{ and } F(\beta, \lambda; y, s) = 0. \quad (43)$$

Thus (43) implicitly defines a function $(\beta, \lambda) = \phi(y, s)$ for $(y, s) \in \mathbb{R}^{p+k}$ near (y_0, s_0) , with $(\beta, \lambda) = \phi(y, s)$ close to (β^*, λ^*) . In particular $\phi(y_0, s_0) = (\beta^*, \lambda^*)$.

- ii. Moreover, the function $\phi : B(r_0; y, s) \rightarrow B(r_1; \beta, \lambda) \subset \mathbb{R}^{p+k}$ above is continuously differentiable, and its derivatives may be determined by differentiating $F(y, s; \phi(y, s)) = 0$ at the solution (β^*, λ^*) to obtain

$$[D_{\beta, \lambda} F(y, s; \beta^*, \lambda^*)] [D_{y, s} \phi(y, s)] = - [D_{y, s} F(y, s; \beta^*, \lambda^*)]. \quad (44)$$

Denoting $F_1 = W \nabla_{\beta} f(\beta; y) + A^T \lambda$ and $F_2 = A\beta - s$, we have

$$D_{\beta, \lambda} F = \begin{pmatrix} W \nabla_{\beta}^2 f(\beta; y) & A^T \\ A & 0_{k \times k} \end{pmatrix}, \quad D_{y, s} F = \begin{pmatrix} W \nabla_{\beta y}^2 f(\beta; y) & 0_{p \times k} \\ 0_{k \times p} & -I_{k \times k} \end{pmatrix}. \quad (45)$$

For separable distance functions f as in all of our examples, the Hessian matrices $\nabla_{\beta}^2 f(\beta; y)$ and $\nabla_{\beta y}^2 f(\beta; y)$ are diagonal. We prune the constraints to ensure A has full rank, so that both $D_{\beta, \lambda} F$ and $D_{y, s} F$ are invertible, and we solve system (44) for $D_{y, s} \phi(y, s)$.

A.6 Nonsmooth Case

The general form of the dual (13) does not require smoothness of f . In the case where f is non-smooth, the form of f^* may require special handling. For example, for the 1-norm loss $\|\beta - y\|_1$, we have

$$f(\beta) = \|\beta - y\|_1 \quad \Leftrightarrow \quad f^*(z) = \delta_{\mathbb{B}_{\infty}}(z) + y^T z, \quad \delta_{\mathbb{B}_{\infty}}(z) := \begin{cases} 0 & |z_i| \leq 1 \quad \forall i \\ \infty & |z_i| > 1 \quad \text{for some } i \end{cases}$$

We can then apply (13) to discover that the dual is a highly structured linear program:

$$\begin{aligned} \mathcal{P} : \quad & \min_{\beta} \|\beta - y\|_1 + c^T \beta \quad \text{s.t.} \quad A\beta = b \\ \mathcal{D} : \quad & \min_{\lambda} \lambda^T (b - Ay) - y^T c \quad \text{s.t.} \quad -1 - c \leq A^T \lambda \leq 1 - c. \end{aligned}$$

In the absence of differentiability, we no longer have (15). However, we can use more general conditions Rockafellar and Wets (2009) to characterize relationships between β^* and λ^* . For example, for the pair of programs above, we have

$$\begin{aligned} -c_i - a_i^T \lambda^* = 1 &\Rightarrow \beta_i^* > y_i \\ -c_i - a_i^T \lambda^* = -1 &\Rightarrow \beta_i^* < y_i \\ | -c_i - a_i^T \lambda^* | < 1 &\Rightarrow \beta_i^* = y_i \end{aligned}$$

which gives rise to a simpler smooth problem with affine equality constraints to obtain the primal solution. In the current paper we focus on smooth losses, relying on (15) to move from the dual to the primal solution.

B Additional Verifications

In this section, we illustrate the raking methods described in Section 2 on simple examples.

B.1 Impact of Raking Loss

To illustrate the effect of the choice of raking loss discussed in Section 2.4 on the final raking values, we generated a 4×5 2D synthetic dataset with observations following a uniform distribution in the interval $[2; 4]$. The sums over the rows are constrained to be equal to 4 and the sums over the columns are constrained to be equal to 5. We use raking weights equal to the inverse of the square of the observations. We first apply raking with the χ -square loss. As no other constraint is applied on the raked values, we note in Figure 6 that some of the raked values are negative. We then apply raking with the entropic loss. The corresponding raked values are then all positive, as where the initial observations. However, we still have raked values lower than 0.5. We finally apply the logistic loss with the lower bounds equal to 0.5 and the upper bounds equal to 4. The raked values are then all contained in the desired interval.

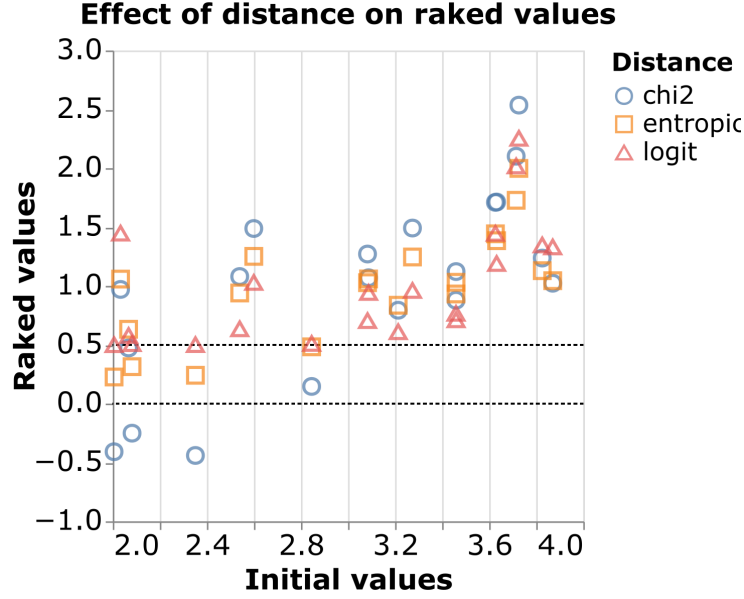


Figure 6: Raked values versus initial values when raking with the χ -square loss (blue circles), the entropic loss (orange squares) and the logistic loss (red triangles). The entropic loss ensures that all raked values remain positive. The logistic loss ensures that all raked values remain bounded in the interval $[0.5; 4]$.

B.2 Impact of Differential Weights

To illustrate the raking weights approach explained in Section 2.5, we rake death rates from two different causes to the all-cause death rate margin, known to be 0.2. For each cause, death rate is computed from 10 observations that follow a binomial distribution. For cause 1, the probability of success p_1 of the binomial distribution is equal to 0.1 and the number of samples varies uniformly between 100 and 200. For cause 2, the observation mechanism is noisy and biased, with probability of success p_2 set to $\text{expit}(\text{logit}(0.1) + \mathcal{N}(0, 0.5))$. Results for 500 simulations are presented in Figure 7. For each simulation, we rake the rate of death without weights and with weights equal to the inverse of the variance of the calculated rates of death. The initial value for cause 1 is centered around its true value 0.1. However, the initial value for cause 2 is overestimated. When raking without weights, both

values are multiplied by the same ratio in order to match the margins value. The raked value for cause 1, which was more certain, is thus farther away from its true value than before the raking process. When raking with weights, the more certain cause 1 is assigned a bigger weight than the more uncertain biased cause 2. After raking, cause 1 stays close to its true value and cause 2 gets closer to its true value than in the case when we rake without weights.

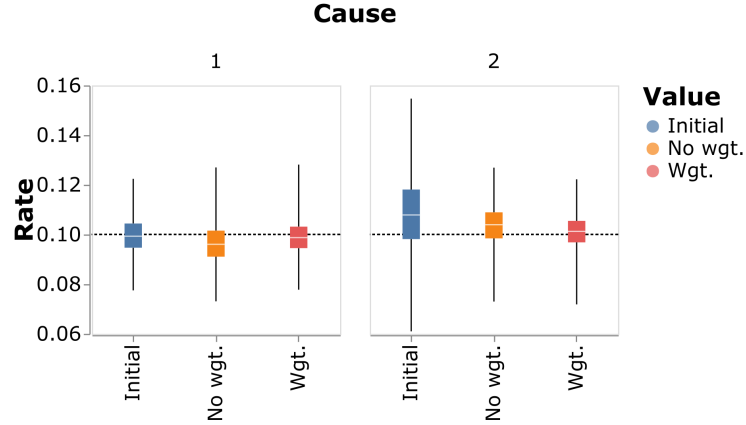


Figure 7: Distribution of initial values (blue), raked values without weights (orange) and raked values with weights (red) for the unbiased cause 1 and the biased cause 2. Adding weights to the raking allows to get a final result closer to the known true value of the rate.

B.3 Using Aggregates as Observations

As an illustration of the use of aggregate observations in the raking explained in Section 2.6, we create a simple $3 \times 4 \times 5$ synthetic example. We fill the table with random values from a uniform distribution over the interval $[0, 10]$. We compute the corresponding margins in each direction, that is we have $3 \times 4 + 3 \times 5 + 4 \times 5 = 47$ margins. Then we add noise to the initial observations by multiplying them with random values from a uniform distribution over the interval $[10, 11]$. We then consider all the observations and margins as initial values to be raked, but we assign a weight of 1 to the observations and bigger

weights to the margins. We try margin weights equal to 1, 2 and 10 times the observation weights. The problem has then $60 + 47 = 107$ unknown raked values and 47 constraints on the partial sums. We then compute the relative error between the noisy values and the initial table and the relative error between the raked values and the initial table. Figure 8 shows the distribution of the relative errors for the noisy data and the raked data. We can see that the raking giving bigger weights to the margins allows us to retrieve the initial table with a small error.

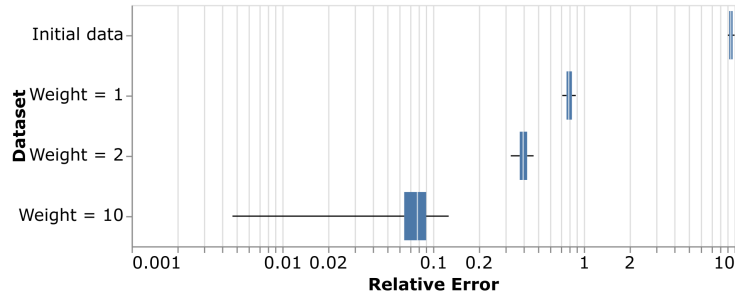


Figure 8: Distribution of the relative errors for the noisy data (top) and for the raked data (bottom, with weights equal to). The raking process with margins given bigger weights than observations allows us to retrieve the initial table.

B.4 Strategies for Missing Data

To illustrate how missing data can be recovered from the raking as explained in Section 2.7, we take a 3D raking example with cardinality $3 \times 4 \times 5$ (i.e. 60 estimates to rake), informed by 3 constraints and 36 aggregate observations. To obtain a baseline rake estimate (no missingness), we rake the initial 60 values using constraints and aggregates. We then remove an entire set of observations for the first dimension, so we have 3 missing observations and one fewer aggregate that corresponds to these.

We are interested in two questions. First, how much do the three missing values affect the raking results for the 57 non-missing values? Second, how well can we recover the three

missing observations (compared to the baseline raked results where none are missing)?

We use four scenarios:

1. Missing values are replaced by 0s and treated as observations.
2. Missing values and their aggregate are treated as missing.
3. Missing values are treated as missing; their aggregate is available.
4. Missing values are replaced by average observations value and assigned a small weight.

In Figure 9, we compared the raked values obtained using these strategies, compared to values we would get when observations are present.

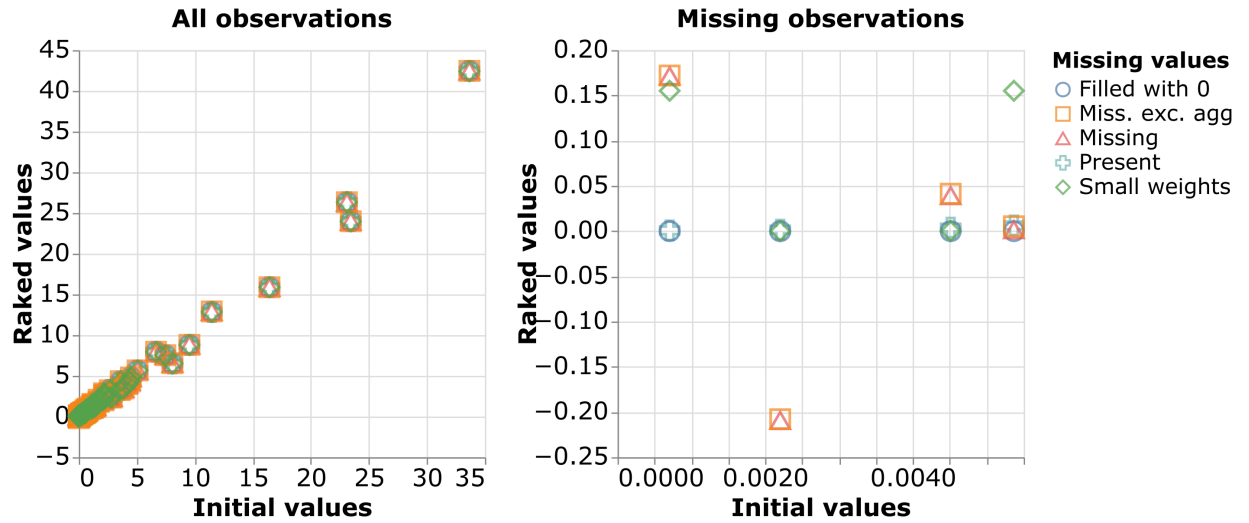


Figure 9: Raked versus initial values when filling the missing values with 0s (blue circles), when computing the missing observations from the other observations and the constraints and the aggregate is present (orange squares) or not present (red triangles), when giving small weights to the missing values (green diamonds) or when no observations are missing (blue crosses). The raked values corresponding to the known observations are only slightly affected by the treatment of the missing values.

First, raked values corresponding to the known observations are essentially unaffected by the strategy for missing values.

Second, we used the entropic distance for the raking, which ensures that the observations present in the data set stay positive after the raking. However, if we treat values as truly missing, there is no entropic loss on them, and hence no guarantee that the recovered missing values will also be positive. Imputing a positive value and assigning small weights to the missing values allows us to impose the positivity conditions.

B.5 Uncertainty Quantification

To illustrate the uncertainty quantification method explained in Section 2.8 and Section A.5, we apply the raking procedure to a small synthetic 2-dimensional example with two categorical variables X_1 and X_2 . We suppose that X_1 can take $m = 3$ values $[1; 2; 3]$ and that X_2 can take $n = 5$ values $[1; 2; 3; 4; 5]$ and we generate $m \times n$ values following a uniform distribution over the interval $[2; 3]$. We compute the margins $s_r = \beta_0 \mathbf{1}_n$ and $s_c = \beta_0^T \mathbf{1}_m$. We then add noise to the balanced table to obtain an unbalanced table $y_0 = \beta_0 + \mathcal{N}(0, 0.1)$. We generate N samples following a multivariate normal distribution with mean y_0 and covariance Σ , with off-diagonal elements equal to 0.01 and diagonal elements set to $\Sigma_{k,k} = 0.1 \times k$ for $k = 1, \dots, m \times n$. We compute the mean \bar{y} of the observations and apply the raking procedure to the mean to get $\beta^* = \phi(\bar{y}, s_1, s_2)$. The results are shown in Figure 10. The blue dots represent the initial observations while the orange squares represent the raked values. The uncertainty on the observations and the raked values is marked by a segment of length two times the standard deviation and centered on the observations or the raked values. In Figure 11 we use the derivative computations (45) to visualize how the initial value of observation $\bar{y}_{3,4}$ affects the corresponding raked values $\beta_{i,j}^*$, and how much the raked value $\beta_{3,4}^*$ depends on the initial observations $\bar{y}_{i,j}$. The intermediate results used to implement the generalized Delta method help to intuitively understand how different estimates affect each other through the raking process. Finally, we compare the uncertainty propagation method described in Section 2.8 to a Monte Carlo method to

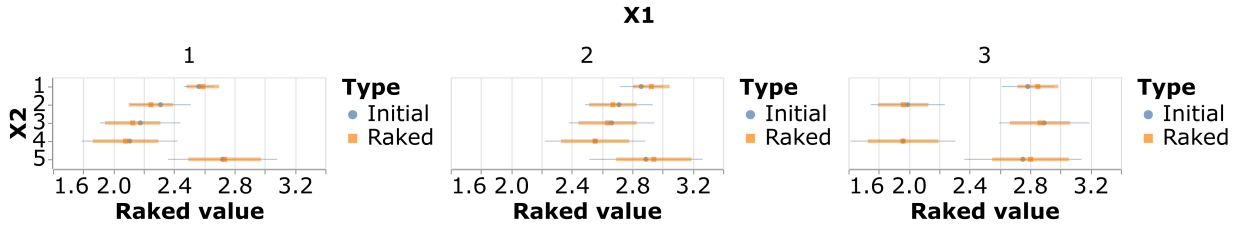


Figure 10: Initial observations (blue dots) and corresponding raked values (orange squares) with their corresponding uncertainties. The raked values are close to the initial observations, but have lower uncertainties as there is no uncertainty on the margins, and marginal constraints help to inform the estimates.

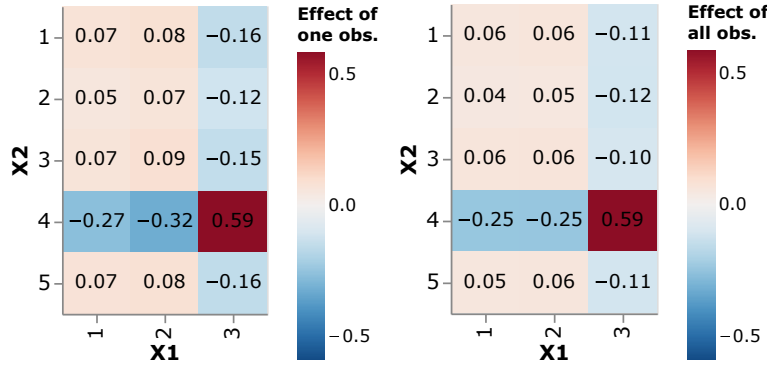


Figure 11: Left panel: Influence of $\bar{y}_{3,4}$ on the raked values. $\beta_{3,4}^*$ is the most positively correlated while $\beta_{3,j}^*$ and $\beta_{i,4}^*$ are negatively correlated. Right panel: Influence of all observations on $\beta_{3,4}^*$. $\bar{y}_{3,4}$ has the strongest positive correlation while $\bar{y}_{3,j}$ and $\bar{y}_{i,4}$ are negatively correlated.

estimate the expectancies and variances of the raked values. For the gold standard, we compute the sample mean and the sample variance of the raked values using 10^6 samples. We then compare in Figure 12 the raked values β^* obtained when raking the expectancy y_0 of the observations and when raking each of the samples $y^{(i)}$ and computing the mean of the raked values, for $N = 100, 1000, 10000, 100000$. We need at least 1000 samples to obtain the same result when raking the samples than when raking the expectancy. We

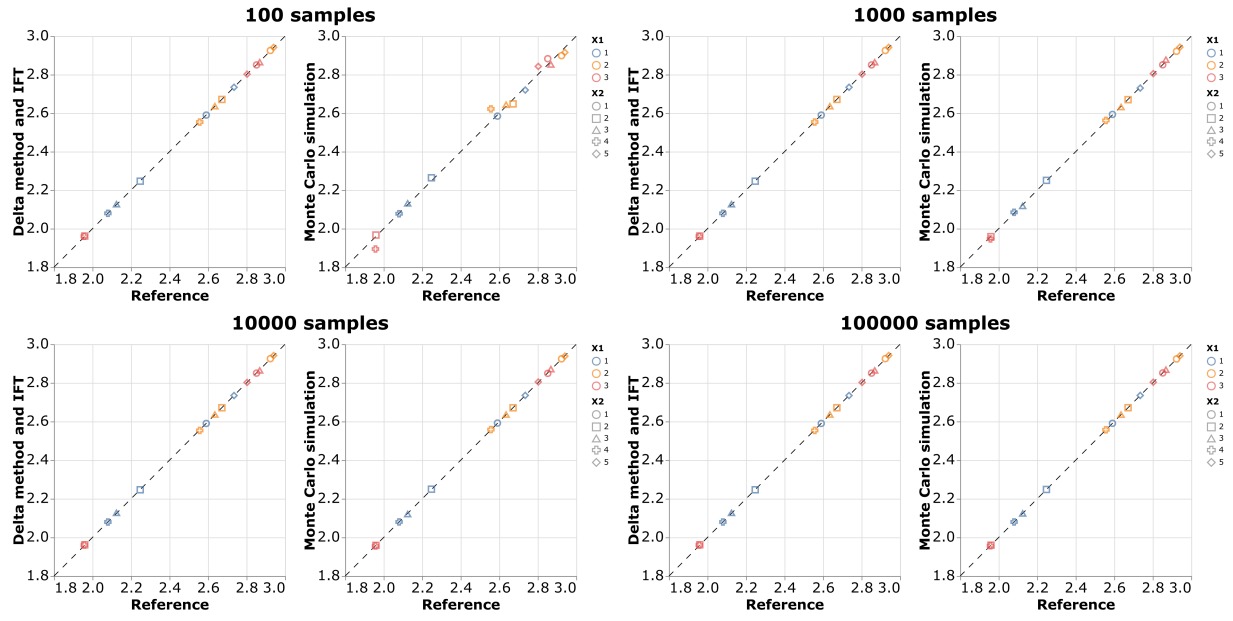


Figure 12: Expectation of the raked values computed with the proposed uncertainty propagation method (left) or with all the samples for $N = 100, 1000, 10000, 100000$ (right, top to bottom). The proposed uncertainty propagation method gives better results than the Monte Carlo method when less than 1000 samples are available.

also compare in Figure 13 the variances of the raked values β^* obtained when raking the expectancy y_0 of the observations (left) and using the uncertainty propagation method and when raking each of the samples $y^{(i)}$ and computing the sample variance of the raked values, for $N = 100, 1000, 10000, 100000$ (right, top to bottom). We need at least 10000 samples to obtain better results when raking the samples than when using the uncertainty propagation method. Our method still has a slight bias compared to the reference. However, in practice we do not expect to have more than a few hundred samples available. Despite the bias, the uncertainty propagation method will then give more accurate results than the Monte Carlo method.

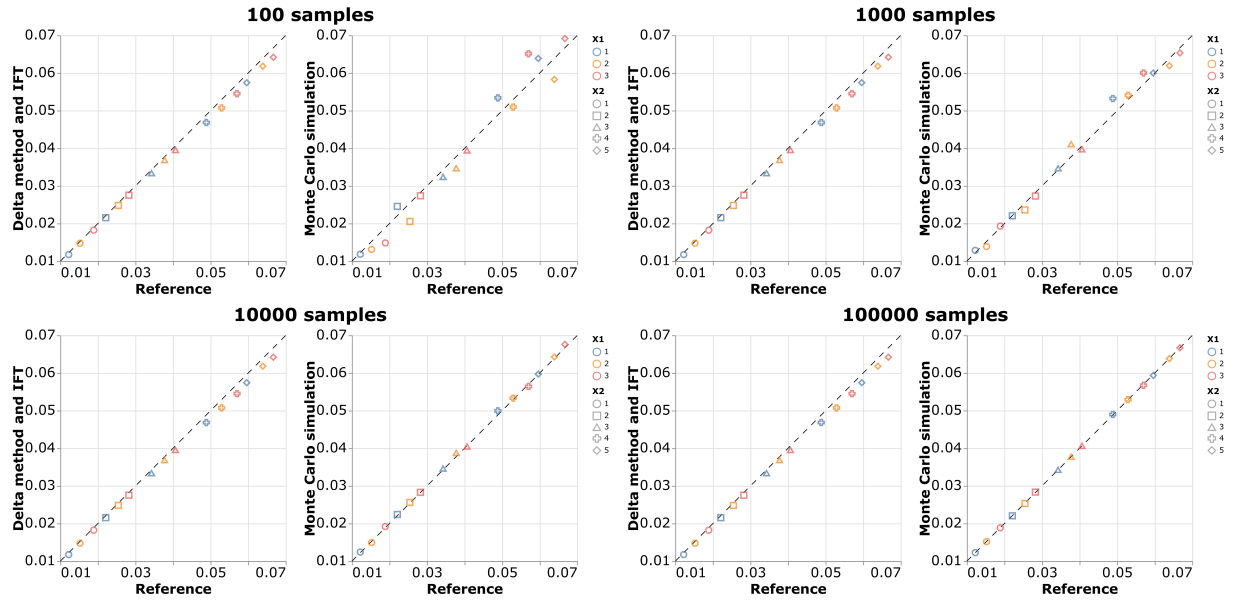


Figure 13: Variance of the raked values computed with the proposed uncertainty propagation method (left) or with all the samples for $N = 100, 1000, 10000, 100000$ (right, left to right). The proposed uncertainty propagation method is close to the Monte Carlo method when the latter uses many samples. More variation is evident in the Monte Carlo results for fewer samples.

C Additional Details for Mortality Rate Estimates

C.1 Comparison of Workflows

In this section, we detail some aspects of the modeling method used for the application of the raking to the mortality estimates described in Section 3.3. The raking problem for mortality estimates can be summarized in Figure 2. In a previous study (Dwyer-Lindgren et al. (2016)), the raking was not done on race and ethnicity. A follow-up study (Dwyer-Lindgren et al. (2023)) used race and ethnicity but without the GBD margins. These studies needed only one- and two-dimensional raking. One-dimensional raking was done using the closed form solution (20) and IPF was used for the two-dimensional raking. To extend Dwyer-Lindgren et al. (2016) and Dwyer-Lindgren et al. (2023) to the case where

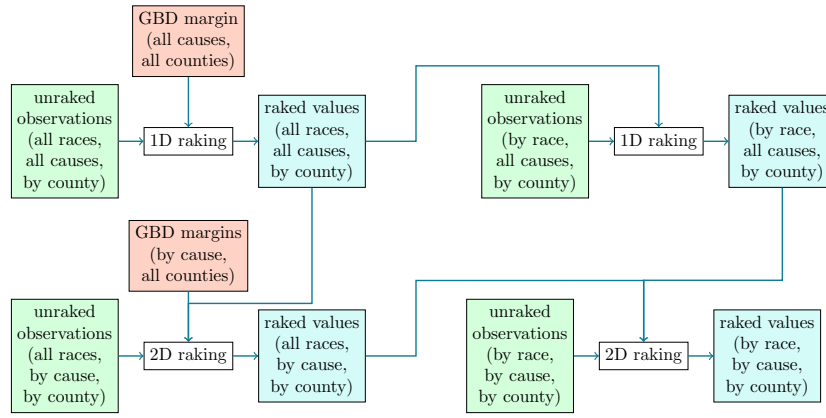


Figure 14: Proposed workflow using only one- and two-dimensional raking to achieve all the internal consistencies between the observations.

raking is done for the three variables cause, race / ethnicity and county, a workflow was first proposed that uses only one- and two-dimensional raking to achieve the requirements described above. The original workflow and the new workflow using the proposed package are summarized in Figures 14 and 15. In Figure 16, we compute the raking procedure for Delaware, both-sex, age group 25-to-30-year-old, using entropic distance and equal weights. We compare the reported values of the death rates (number of deaths divided by the population for each race and county) with the corresponding raked values for both workflows for all 72 cases (3 counties, 5 races and all races, 3 causes and all causes). The 1-step approach gives raked values slightly closer to the initial values than the 4-steps workflow, meaning that the raked estimates stay closer to the original reported values while satisfying the requirements. This improvement is easier to see for larger reported death rates on the linear scale plot in Figure 16.

C.2 Additional Results

We show in Figures 17 and 18 the initial and raked values with associated uncertainty ordered by cause and race.

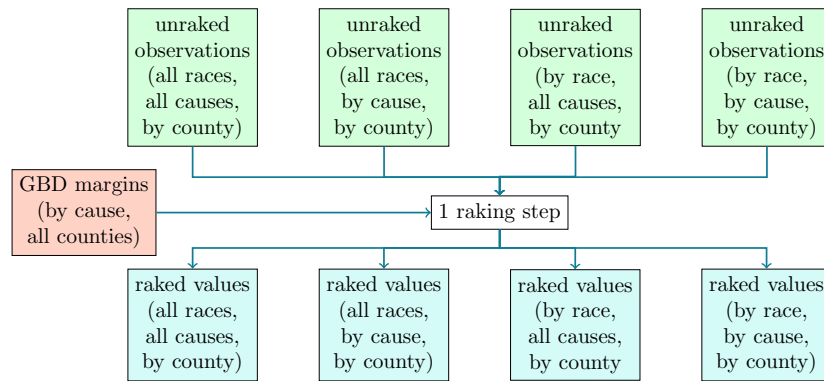


Figure 15: Proposed workflow using only one- and two-dimensional raking to achieve all the internal consistencies between the observations.

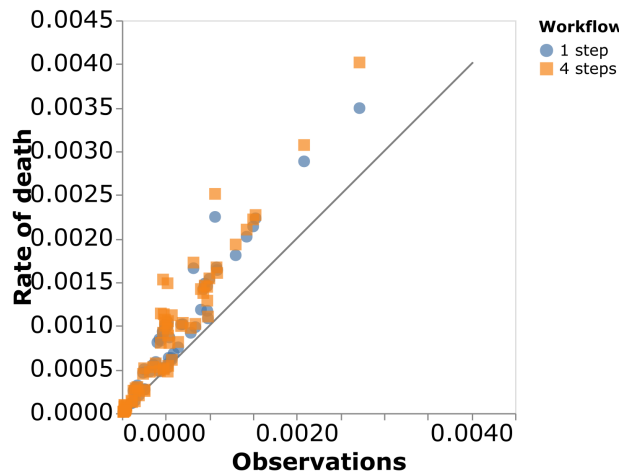


Figure 16: Raked values vs initial rate of death for the two proposed workflows for Delaware, age group 25-30. The raked values obtained with the proposed 1-step workflow are usually closer to the initial observations than the raked values obtained with the previous 4-step workflow.

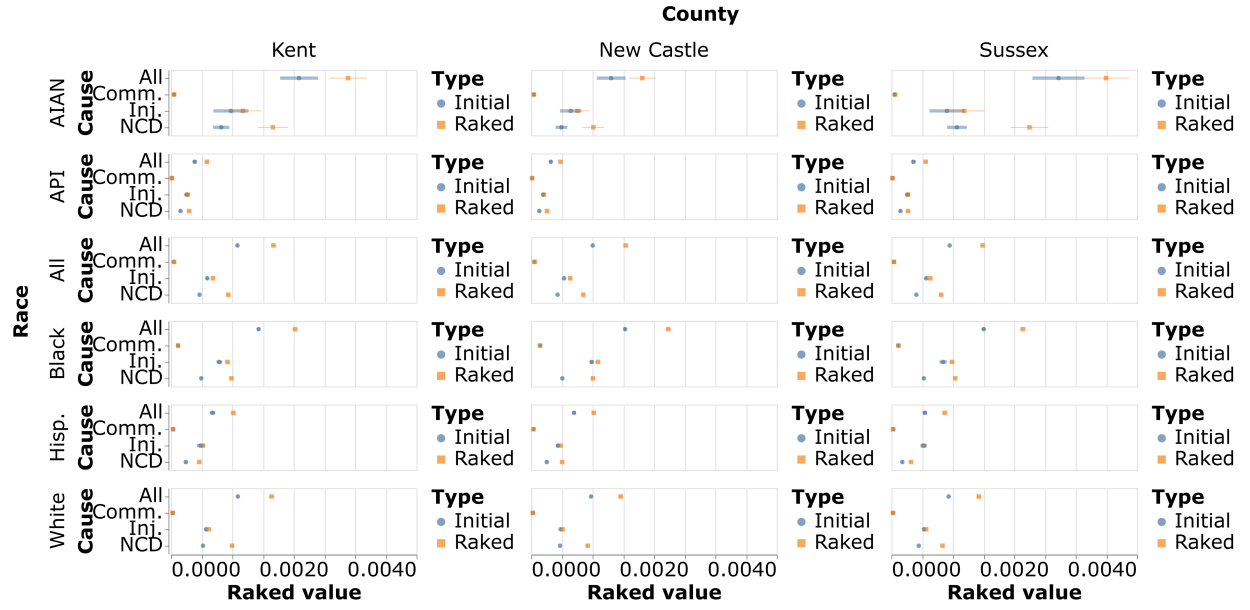


Figure 17: Initial and raked values with associated uncertainty ordered by cause. The raked values are close to the initial observations, but have smaller uncertainties, as the uncertainty on the margins is smaller than the uncertainty reported for the observations.

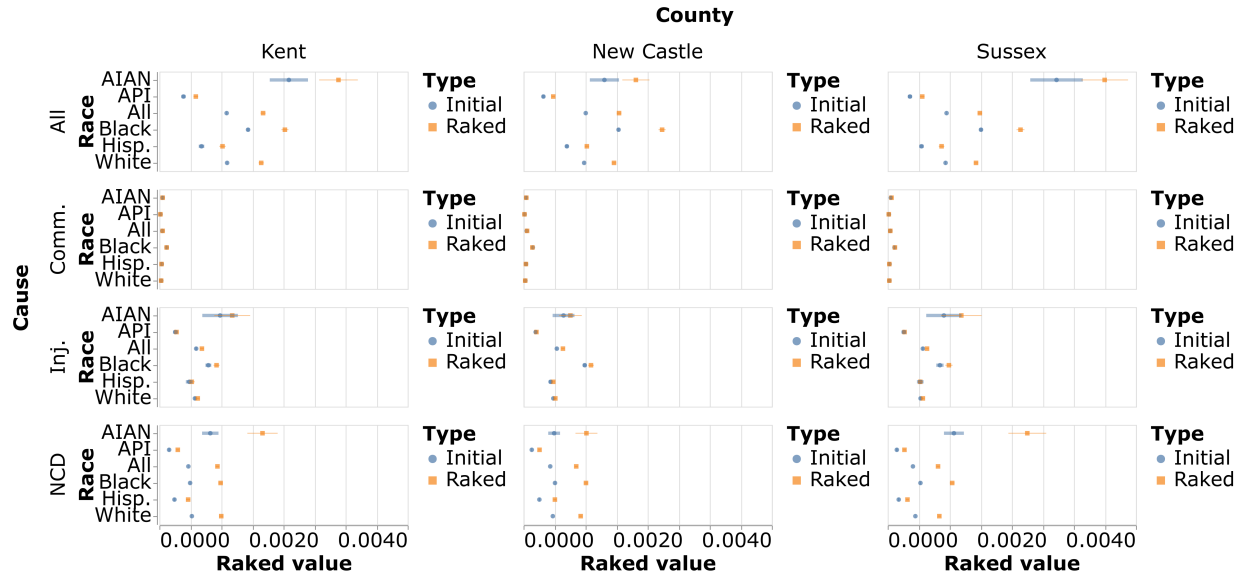


Figure 18: Initial and raked values with associated uncertainty ordered by race. The raked values are close to the initial observations, but have smaller uncertainties as the uncertainty on the margins is smaller than the uncertainty reported for the observations.

C.3 Influence of Observations on Raked Values

Using the intermediate derivative results, we can visualize which observation points have the most influence on the final estimated raked values. We look at the raked value for cause “injuries”, race group White and New Castle County (denoted $\beta_{2,1,2}$). Then we compute the corresponding values of the gradient $\frac{\partial \beta_{2,1,2}}{\partial y_{i,j,k}}$ and $\frac{\partial \beta_{2,1,2}}{\partial s_i}$ for $i = 0, \dots, 3$, $j = 0, \dots, 5$ and $k = 1, 2, 3$. The corresponding values of the gradient are shown in Figure 19. The most important observation point is the one with the same cause, race and county as the raked value considered. Increases in all causes and all races deaths will increase the raked value, while increases in other causes and races will decrease it. The initial values for the other counties will have a smaller influence on the raked value. For the margins, increase in all races state mortality due to injuries will increase the raked value. An increase in all races state mortality due to communicable diseases decreases the raked value, while an increase in all races state mortality due to non-communicable diseases increases the raked value as a result of increasing all cause deaths.

References

- Causes of Death Collaborators (2018), “GBD 2017 . Global, regional, and national age-sex-specific mortality for 282 causes of death in 195 countries and territories, 1980–2017: a systematic analysis for the Global Burden of Disease Study 2017,” *Lancet*, 392, 1736–88.
- Cuturi, M. (2013), “Sinkhorn distances: Lightspeed computation of optimal transport,” *Advances in neural information processing systems*, 26.
- Deming, W. E., and Stephan, F. F. (1940), “On a least squares adjustment of a sampled frequency table when the expected marginal totals are known,” *The Annals of Mathematical Statistics*, 11, 427–444.

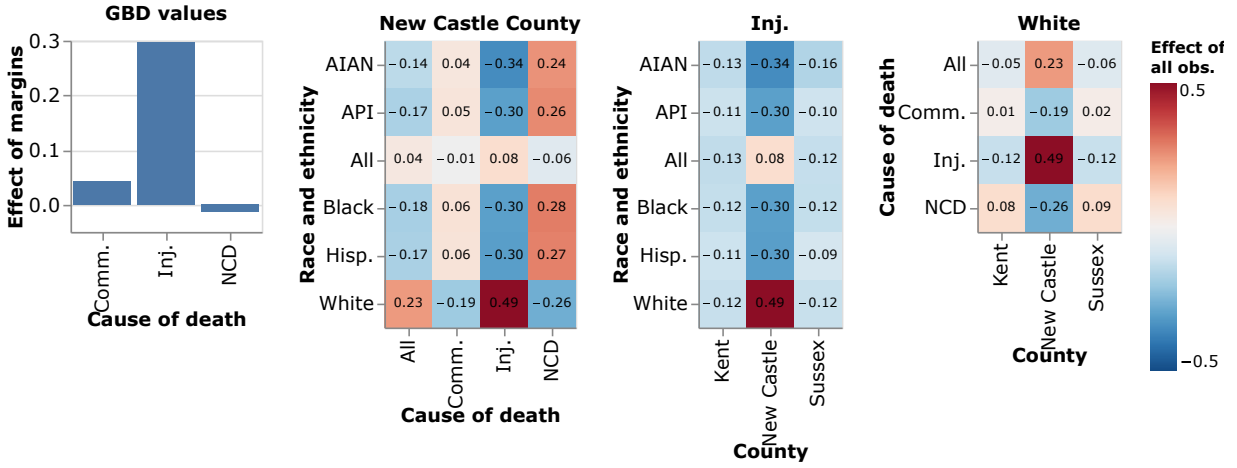


Figure 19: Influence of all the initial values and aggregated initial values on the raked value for cause injuries, race group White and New Castle County. As expected, the corresponding observation $\bar{y}_{2,1,2}$ is the most influential, followed by the margin for the cause “injuries”.

Devaud, D., and Tillé, Y. (2019), “Deville and Särndal’s calibration: revisiting a 25-years-old successful optimization problem,” *Test*, 28, 1033–1065.

Deville, J.-C., and Särndal, C.-E. (1992), “Calibration estimators in survey sampling,” *Journal of the American Statistical Association*, 87, 376–382.

Deville, J.-C., Särndal, C.-E., and Sautory, O. (1993), “Generalized raking procedures in survey sampling,” *Journal of the American Statistical Association*, 88, 1013–1020.

Dwyer-Lindgren, L., Bertozzi-Villa, A., Stubbs, R. W., Morozoff, C., Kutz, M. J., Huynh, C., Barber, R. M., Shackelford, K. A., Mackenbach, J. P., van Lenthe, F. J., Flaxman, A. D., Naghavi, M., Mokdad, A. H., and Murray, C. J. L. (2016), “US county-level trends in mortality rates for major causes of death, 1980-2014,” *JAMA : the journal of the American Medical Association*, 316, 2385–2401.

Dwyer-Lindgren, L., Kendrick, P., Kelly, Y. O., Baumann, M. M., Compton, K., Blacker,

- B. F., Daoud, F., Li, Z., Mouhanna, F., Nassereldine, H., Schmidt, C., Sylte, D. O., Hay, S. I., Mensah, G. A., Nápoles, A. M., Pérez-Stable, E. J., Murray, C. J., and Mokdad, A. H. (2023), “Cause-specific mortality by county, race, and ethnicity in the USA, 2000-19: a systematic analysis of health disparities,” *The Lancet*, 402, 1065–108.
- Folland, G. B. (2002), *Advanced calculus*, Upper Saddle River, NJ: Prentice Hall.
- Horvitz, D., and Thompson, D. (1952), “A generalization of sampling without replacement from a finite universe,” *Journal of the American Statistical Association*, 47, 663–685.
- Kim, J. K., Fuller, W. A., and Bell, W. R. (2011), “Variance estimation for nearest neighbor imputation for US Census long form data,” *The Annals of Applied Statistics*, 5, 824–842.
- Lu, H., and Gelman, A. (2003), “A method for estimating design-based sampling variances for surveys with weighting, poststratification, and raking,” *Journal of Official Statistics*, 19, 133–151.
- Moretti, A., and Whitworth, A. (2023), “Estimating the uncertainty of a small area estimator based on a microsimulation approach,” *Sociological Methods & Research*, 52, 1785–1815.
- Narain, R. (1951), “On sampling without replacement with varying probabilities,” *Journal of the Indian Society of Agricultural Statistics*, 3, 169–174.
- Rockafellar, R. T., and Wets, R. J.-B. (2009), *Variational analysis*, vol. 317, Springer Science & Business Media.
- She, Y., and Tang, S. (2019), “Iterative proportional scaling revisited: A modern optimization perspective,” *Journal of Computational and Graphical Statistics*, 28, 48–60.
- Si, Y., and Zhou, P. (2021), “Bayes-raking: Bayesian finite population inference with known margins,” *Journal of Survey Statistics and Methodology*, 9, 833–855.

- Sinkhorn, R. (1967), “Diagonal equivalence to matrices with prescribed row and column sums,” *The American Mathematical Monthly*, 74, 402–405.
- Stephan, F. F. (1942), “An iterative method of adjusting sample frequency tables when expected marginal totals are known,” *The Annals of Mathematical Statistics*, 13, 166–178.
- Tillé, Y. (2020), *Sampling and estimation from finite populations*, Newark: John Wiley & Sons, Incorporated.
- Williams, M. R., and Savitsky, T. D. (2024), “Optimization for calibration of survey weights under a large number of conflicting constraints,” *Journal of Computational and Graphical Statistics*, 33, 1047–1060.